1   Dryopithecine palaeobiodiversity in the Iberian Miocene revisited on the basis of

2   molar endostructural morphology

3

4   *by* JOSEP FORTUNY[1*], CLÉMENT ZANOLLI[2], FEDERICO BERNARDINI[3,4],

5   CLAUDIO TUNIZ[3,4,5] *and* DAVID M. ALBA[1,*]

6

7   [1] Institut Català de Paleontologia Miquel Crusafont, Universitat Autònoma de

8   Barcelona, Edifici ICTA-ICP, C/ Columnes s/n, Campus de la UAB, 08193

9   Cerdanyola del Vallès, Barcelona, Spain; emails: josep.fortuny@icp.cat (ORCiD:

10   0000-0003-4282-1619), david.alba@icp.cat (ORCiD: 0000-0002-8886-5580)

11   [2] Laboratoire PACEA, UMR 5199 CNRS, Université de Bordeaux, Pessac, France;

12   email: clement.zanolli@gmail.com (ORCiD: 0000-0002-5617-1613)

13   [3] Department of Humanistic Studies, Università Ca'Foscari, Venezia,

14   Italy

15   [4] Multidisciplinary Laboratory, the 'Abdus Salam' International Centre for Theoretical

16   Physics, Via Beirut 31, 34151 Trieste, Italy; emails: fbernard@ictp.it (ORCiD: 0000-

17   0002-3282-8799), ctuniz@ictp.it (ORCiD: 0000-0001-6582-7568)

18   [5] Center for Archaeological Science, University of Wollongong, Northfields Ave,

19   Wollongong, NSW 2522, Australia

20

21   * Corresponding authors.

22

23   **Abstract:** Extensive fieldwork at Abocador de Can Mata (NE Iberian Peninsula) has

24   uncovered a previously unsuspected diversity of catarrhine primates in the middle

25   Miocene (12.5–11.6 Ma) of Europe. However, the distinction of the great ape genera

26 *Pierolapithecus* and *Anoiapithecus* from *Dryopithecus*—supported by craniodental

27 differences—has been disputed by some authors. Here we revisit the diversity of great

28 apes (dryopithecines) from the Iberian Miocene based on molar 3D endostructural

29 morphology (relative enamel thickness, enamel distribution, and enamel-dentine

30 junction [EDJ]). Using microtomography, we inspected an extensive sample of 49

31 hominoid molars representing at least five species from 12 localities. 2D and 3D

32 relative enamel thickness values indicate that *Dryopithecus* and "*Sivapithecus*"

33 *occidentalis* (species inquirenda) display the thinnest and thickest enamel,

34 respectively, while the remaining taxa (*Hispanopithecus, Anoiapithecus,*

35 *Pierolapithecus*) show intermediate values. Upper molar enamel distribution maps

36 exhibit a similar pattern in *P. catalaunicus*, *A. brevirostris*, *D. fontani*, *H. laietanus*

37 and *H. crusafonti* whereas for the lower molars they reveal differences between

38 *Hispanopithecus laietanus* and *Hispanopithecus crusafonti*. Lower molar enamel

39 distribution and EDJ morphology of "*S.*" *occidentalis* support the distinction of this

40 species but do not resolve if it is a junior synonym of *Anoiapithecus brevirostris* or

41 *Pierolapithecus catalaunicus*. Overall our results support the distinction of middle

42 Miocene dryopithecins from late Miocene hispanopithecins, the distinction of

43 *Pierolapithecus* and *Anoiapithecus* from *Dryopithecus* among the former, and the

44 distinct species status of *H. crusafonti* compared to *H. laietanus* among the latter. Our

45 results highlight the potential of inner tooth morphology for hominoid alpha-

46 taxonomy.

47

48 **Key words:** Fossil primates; Hominoidea; Dryopithecinae; Dental morphology;

49 Enamel-dentine junction; Relative enamel thickness

50

The Miocene record of great apes (Primates: Hominidae) in the Iberian Peninsula is restricted to Catalonia in NE Spain (Vallès-Penedès and Seu d'Urgell basins) (Casanovas-Vilar *et al.* 2011; Alba 2012). Until two decades ago, all great apes from the Iberian Miocene were subsumed into a single genus, *Dryopithecus* (e.g., Begun *et al.* 1990; Harrison 1991; Begun 1992, 2002, 2007; Moyà-Solà & Köhler 1993, 1995; Ribot *et al.* 1996), although most of the available sample consisted of late Miocene remains (Golpe Posse 1993). Since 2002, new discoveries at the middle to late Miocene Abocador de Can Mata (ACM) composite section (ca. 12.6–11.4 Ma) (Alba *et al.* 2006, 2017; Casanovas-Vilar *et al.* 2011, 2016) have unveiled a previously unsuspected diversity of catarrhine primates (Alba 2012; Alba *et al.* 2017), including pliopithecoids (Alba *et al.* 2010*a*, 2012*a*), the small-bodied putative stem hominoid *Pliobates* (Alba *et al.* 2015), and as many as three great ape (hominid) genera, each represented by a single species: *Pierolapithecus catalaunicus* (Moyà-Solà *et al.* 2004), *Anoiapithecus brevirostris* (Moyà-Solà *et al.* 2009*a*; Alba *et al.* 2013), and *Dryopithecus fontani* (Moyà-Solà *et al.* 2009*b*; Alba & Moyà-Solà 2012)—of which the two former were originally described based on ACM material (Moyà-Solà *et al.* 2004, 2009*a*).

An isolated upper molar from els Hostalets de Pierola assigned to *Dryopithecus* by van der Made & Ribot (1999) most likely comes from younger levels than those recorded at ACM (Alba et al. 2013). Although this specimen was left unassigned to genus in some previous publications (e.g., Alba 2012; Alba *et al.* 2013), it is here attributed to *D. fontani* following Alba *et al.* (2020). In turn, a mandibular fragment from ACM is provisionally assigned to "*Sivapithecus*" *occidentalis* (Alba *et al.* 2020). This nominal species is currently recognized as a species inquirenda because it differs from *D. fontani* but additional material would be required to discount an attribution to

76 either *P. catalaunicus* or *A. brevirostris* (Alba *et al.* 2020). The recovery of cranial

77 remains assigned to *Dryopithecus* at ACM also prompted the resurrection of genus

78 *Hispanopithecus* (Moyà-Solà *et al.* 2009*b*) and the transferral into it of two late

79 Miocene great ape species from the Vallès-Penedès Basin (*Hispanopithecus laietanus*

80 and *Hispanopithecus crusafonti*; see Begun 1992, 2002; Moyà-Solà & Köhler, 1993,

81 1995; Golpe Posse 1993; Alba *et al.* 2012*b*) formerly assigned to *Dryopithecus* (see

82 references above). All these genera are generally considered to belong to a single

83 group, here distinguished as the subfamily Dryopithecinae (Alba 2012), whose

84 phylogenetic affinities are still unclear—being generally considered either stem

85 hominids (Moyà-Solà *et al.* 2004, 2009*a*; Alba 2012; Alba *et al.* 2015) or hominines

86 (Begun 2009, 2015; Begun *et al.* 2012). The distinction of two species of

87 *Hispanopithecus* (Begun 1992; Cameron 1999; Alba *et al.* 2012*b*), formerly criticized

88 by several authors (Harrison 1991; Andrews *et al.* 1996; Ribot *et al.* 1996), also relies

89 on dental differences and therefore requires more detailed studies.

90   While the distinction of *Hispanopithecus* is currently universally accepted

91 (Casanovas-Vilar *et al.* 2011; Alba 2012; Begun *et al.* 2012; Alba *et al.* 2012*b*, 2015;

92 Begun 2015; Böhme *et al.* 2019), the recognition of three middle Miocene

93 dryopithecine genera in the Vallès-Penedès Basin (Casanovas-Vilar *et al.* 2011; Alba

94 2012; Alba & Moyà-Solà 2012; Alba *et al.* 2013, 2020; Pérez de los Ríos *et al.* 2013;

95 Marigó *et al.* 2014) has been accepted by some (Pickford 2012; Fleagle 2013; Böhme

96 *et al.* 2019; Andrews 2020) but questioned by others (Begun 2009, 2010, 2015). In

97 particular, both *Pierolapithecus* and *Anoiapithecus* have been considered likely junior

98 synonyms of *Dryopithecus* (Begun 2009). Although the distinction of the former is

99 mainly based on cranial anatomy (Moyà-Solà *et al.* 2004, 2009*a,b*; Alba 2012; Pérez

100 de los Ríos *et al.* 2012), subtle differences in dental morphology have also been argued

101   to differentiate these two genera among themselves and relative to both *Dryopithecus*

102   and *Hispanopithecus* (Alba & Moyà-Solà 2012; Alba *et al.* 2013, 2020; Pérez de los

103   Ríos *et al.* 2013). Although the postcranial record is more restricted (unknown for

104   *Anoiapithecus*), it also supports the genus distinction between *Pierolapithecus* and

105   *Hispanopithecus* (Moyà-Solà *et al.* 2004, 2005; Almécija *et al.* 2007, 2009; Alba *et al.*

106   2010*c*, 2011, 2012*c*) and hints at some differences between *Dryopithecus* and the two

107   former genera (Moyà-Solà *et al.* 2009*b*; Almécija *et al.* 2013; Pina *et al.* 2012, 2019).

108   Enamel thickness variation (Alba *et al.* 2010*b*, 2013, 2020) and, most recently,

109   crown endostructural variation (Alba *et al.* 2020) have also been investigated to clarify

110   the allocation of fragmentary dentognathic remains (Alba *et al.* 2020). A large

111   proportion of hominoid specimens from the Vallès-Penedès Basin are fragmentary

112   denthognatic remains or isolated teeth. Therefore, dental morphology plays a very

113   important role in the alpha-taxonomy of these taxa. Unfortunately, taxonomic

114   assessments based on dental morphology on Iberian dryopithecines are complicated by

115   small sample sizes and overall similarities in occlusal morphology. Non-invasive

116   techniques based on X-ray microcomputed tomography (μCT) provide a wealth of

117   additional information on the inner structural morphology of teeth (Macchiarelli *et al.*

118   2013), which complements and augments that provided by the outer enamel surface

119   (OES). The latter is often affected by occlusal wear or taphonomic damages. In

120   contrast, μCT grants non-destructive access to tooth endostructural morphology and

121   enables the assessment of taxonomic and functionally-related parameters such as

122   enamel thickness distribution over the crown, as well as enamel-dentine junction

123   (EDJ) shape.

124   To test the hypotheses that the Iberian Miocene hominid diversity includes at least

125   four genera (*Pierolapithecus*, *Anoiapithecus*, *Dryopithecus*, *Hispanopithecus*) and

126 further evaluate the taxonomic distinctiveness of these Miocene dryopithecines from

127 Catalonia, we investigate the internal dental morphology based on most of the

128 available upper and lower molars. Enamel thickness, previously investigated for the

129 middle Miocene (Alba *et al.* 2010*b*, 2013, 2020) and late Miocene (Andrews & Martin

130 1991; Smith *et al.* 2019) dryopithecines, is here analyzed in 2D and, for the first time,

131 in 3D. We also describe the EDJ morphology of these taxa in relation to previous

132 observations based on OES morphology, and based on these data we reevaluate the

133 distinction between the investigated dryopithecine taxa. Based on the previously

134 published research cited above, differences in terms of dental endostructural

135 organization are to be expected between (1) middle Miocene and late Miocene

136 hominoids; (2) *Dryopithecus* as compared with *Pierolapithecus* and *Anoiapithecus*

137 (and "*S.*" *occidentalis*), particularly in terms of tissue proportions; and (3) *H.*

138 *crusafonti* and *H. laietanus*, with the latter being somewhat more derived relative to

139 the middle Miocene genera.

140

141 **MATERIAL AND METHODS**

142 *Dental terminology*

143   The dental terminology employed in the descriptions is depicted in Fortuny *et al*.

144 (2020, fig. 1). It follows that of Harrison and Gu (1999), except that 'protoconule' is

145 favored over 'paraconule' (Swindler 2002).

146

147 *Studied sample*

148   It consists of 49 (30 upper and 19 lower) permanent molars from 25 specimens

149 representing a minimum of 15 individuals from 12 localities—see Table 1 for

150 provenance details. The specimens are housed at the Institut Català de Paleontologia

151 Miquel Crusafont, Sabadell, Spain (acronym IPS), except for two specimens housed at

152 the Museu de Geologia del Seminari de Barcelona, Spain (MGSB).

153

154 *Computational techniques*

155 *Microcomputed tomography acquisitions* Specimens were imaged by microfocus X-

156 ray microcomputed tomography (µCT) at the Multidisciplinary Laboratory of the

157 'Abdus Salam' International Centre for Theoretical Physics of Trieste. The scans were

158 made with a transportable scanner specifically designed for the investigation of

159 cultural heritage items. X-rays are produced by a Hamamatsu microfocus X-ray source

160 (150 kV maximum voltage, 500 mA maximum current, and 5 mm minimum focal spot

161 size) and the detector is a Hamamatsu CMOS flat panel coupled to a fibre optic plate

162 under the GOS scintillator. The system has been designed to allow large sample-to-

163 detector distances to exploit phase-contrast effects (Tuniz *et al.* 2013). The

164 acquisitions were performed according to the following parameters: 120 to 150 kV

165 voltage; 62 to 201 µA current; a projection each 0.15° to 0.20° (see Fortuny *et al*.

166 (2020, table 1 for details). MicroCT raw data requests should be addressed to the

167 Fieldwork & Collection Management Area of the ICP.

168

169 *Virtual reconstruction and segmentation* The final volumes were reconstructed using

170 Cobra v.7.4.16 (Exxim) and DigiCT v.2.3.3 (DIGISENS) in 8-bit format, with an

171 isotropic voxel size ranging from 14.36 to 20.42 µm (see Fortuny *et al*. 2020, table 1

172 for details). Using Avizo 7.0 (FEI-Visualization Sciences Group Inc.) and ImageJ

173 v.1.47 (NIH; Schneider *et al.* 2012), a semiautomatic threshold-based segmentation

174 was carried out (Fortuny *et al*. 2020, fig. 2) following the half-maximum height

175 method (HMH; Spoor *et al.* 1993) and the region of interest thresholding protocol

176   (ROI-Tb; Fajardo *et al.* 2002), taking repeated measurements on different slices of the

177   virtual stack (Coleman & Colbert 2007).

178   Digital surface models of the OES and EDJ of the investigated molars are available on

179   MorphoSource (www.morphosource.org). OES models are openly shared from

180   Morphosource, whereas the EDJ are available through Morphosource upon request;

181   see Fortuny *et al.* 2020, table 2 for digital object identifiers and further details.

182

183   *Relative enamel thickness* 2D relative enamel thickness (RET) was computed

184   following a protocol originally devised for histological sections (Martin 1985). In

185   order not to overestimate RET due to obliquity, it was assessed on virtual coronal

186   buccolingual sections perpendicular to the best-fit plane of the cervical line and

187   passing through the tips of the mesial dentine horns (Benazzi *et al.* 2014). This method

188   was already used in previous studies to compute 2D RET values for the middle

189   Miocene specimens included in this study (Alba *et al.* 2013, 2020). The following

190   formula was employed (Martin 1985; Smith *et al.* 2005; Alba *et al.* 2010*b*): 2D RET =

191   2D AET $\times$ 100 / b$^{1/2}$, wherein b is the dentine and pulp area, 2D AET is average

192   enamel thickness, computed as 2D AET = c (enamel cap area) / e (enamel-dentine

193   junction length). While 2D RET is a dimensionless variable originally developed to

194   compare enamel thickness among species of different tooth size (Martin 1985), the

195   assessment of intraindividual intertooth variation should instead be based on 2D AET

196   (Smith *et al.* 2005). As done by other authors (e.g., Smith *et al.* 2005), for several of

197   the analyzed teeth it was necessary to correct RET calculations for tooth wear. As it is

198   frequently done to maximize the sample available for the estimation of tissue

199   proportions (e.g., Smith *et al.* 2006, 2012*a*; Martin-Francés *et al.* 2018),

200   reconstructions of the worn enamel and dentine horn tip were made prior to

201 measurement for sections showing light to moderate wear, or when a small amount of

202 cervical enamel was missing (based on the curvature and orientation of the outer

203 enamel surface relative to the EDJ). Tooth wear stages were assessed following the

204 adaptation of a previous protocol established on human teeth (Smith 1984). Specimens

205 that were too heavily worn (above stage 4) were excluded. In consequence, a total of

206 41 specimens (25 upper molars and 16 lower molars) were analyzed for 2D RET. The

207 formulas employed to compute 3D AET and 3D RET are just the three-dimensional

208 extension of those employed to compute 2D RET (Olejniczak 2006; Olejniczak *et al.*

209 2008*a*,*b*,*c*,*d*; Benazzi *et al.* 2014): 3D AET = Ve / SEDJ and 3D RET = 3D AET $\times$

210 100 / Vcdp$^{1/3}$, wherein Ve is enamel cap volume, Vcdp is dentine and pulp volume,

211 and SEDJ is EDJ surface area. A total of 31 specimens (21 upper molars and 10 lower

212 molars) were analyzed for 3D RET.

213   We refrained from using discrete categorizations of enamel thickness stemming

214 from the thin vs. thick dichotomy (Martin 1985) in considering that they do not

215 adequately reflect either the continuum displayed among different teeth of a single

216 individual or intra- and interpecific variability. Therefore, comparisons between the

217 analyzed Miocene apes and other hominoids were based on statistical comparisons of

218 2D RET and 3D RET values among species. For 2D RET results we also included in

219 the statistical comparisons the data derived from the histological sections used by

220 Andrews & Martin (1991) and Kelley *et al.* (2001) as reported by Smith *et al.* (2019).

221 The small available sample sizes precluded performing statistial tests to assess

222 differences in RET for different tooth loci separately, as such comparisons would not

223 have enough statistical power to denote significant differences. Statistical comparisons

224 were instead done by lumping the data from all tooth loci. These comparisons should

225 be taken with great care because there is a trend towards increasing relative enamel

226 thickness from first to third molars in both humans and apes (Grine & Martin 1988;

227 Macho 1994; Grine 2002, 2005; Smith *et al.* 2005, 2006, 2019). To account for this

228 problem, we compared individual data for Vallès-Penedès hominoids with the median

229 values and range of variation displayed by extant great ape genera for each tooth locus

230 separately (Smith *et al.* 2008, 2012*b*, 2019). Comparisons of 2D RET and 3D RET

231 values for both extant and extinct taxa were made with PAST v. 4.01 (Hammer *et al.*

232 2001) by means of Kruskal-Wallis tests for equality of medians and pairwise Mann-

233 Whitney post hoc comparisons, which are non-parametric and hence do not assume

234 normal distributions, with and without Bonferroni correction. Adjusted z-score

235 analyses were performed for 2D RET and 3D RET from the Iberian Miocene great

236 apes and on five extant comparative taxa. This method allows the comparison of

237 unbalanced samples, as it is often the case in the fossil record.

238

239 *Enamel distribution maps* Enamel distribution maps permit comparisons in the local

240 distribution of enamel over the entire crown surface (Macchiarelli *et al.* 2008, 2009,

241 2013; Zanolli *et al.* 2019; Thiery *et al.* 2017). Enamel thickness topographic variation

242 was rendered for 44 specimens (25 upper molars and 19 lower molars) through 3D

243 cartographies using a chromatic scale where thickness increases from dark blue (thin)

244 to red (thick) (Macchiarelli *et al.* 2008, 2013; Bayle *et al.* 2011). The software Avizo

245 7.0 (FEI-Visualization Sciences Group Inc.) was used for this purpose. This

246 visualization technique maps the local enamel thickess by computing the site-specific

247 shortest distance between the OES and EDJ surfaces.

248

249 *EDJ morphology* The morphology of the EDJ was examined in the same 44

250 specimens. The Miocene hominid molars exhibit expression of non-metric features

251   that are not covered with the usual scoring systems like the Arizona State University

252   Dental Anthropology method that was developed for human/hominin teeth (Turner *et*

253   *al.* 1991; Scott & Irish 2017). Therefore, we elaborated a qualitative approach based

254   on a limited number of stages for each feature (see descriptions of traits in the Tables 3

255   and 4).

256

257   **RESULTS**

258   *Enamel thickness*

259   2D RET was computed for 41 specimens (see Fortuny *et al*. 2020, table 3 and

260   sections used in Fortuny *et al*. 2020, figs 3–5). 2D RET values for 20 specimens,

261   attributed to *P. catalaunicus*, *A. brevirostris*, *D. fontani* and "*S.*" *occidentalis*, had

262   already been published (see Alba *et al.* 2013, 2020), while 3D RET was newly

263   reported for 31 specimens (see Fortuny *et al*. (2020, table 4).

264   Based on average 2D RET values (Table 2, Fig. 1 A; see Fortuny *et al*. 2020, table

265   5 and figs 6, 7A), *D. fontani* displays the thinnest enamel (12.3), while "*S.*"

266   *occidentalis* displays the thickest (19.6) among analyzed sample, and other

267   dryopithecines display similar intermediate average values; in order of increasing 2D

268   RET: *H. laietanus* (14.3), *H. crusafonti* (14.4), *A. brevirostris* (14.6), and *P.*

269   *catalaunicus* (15.4). Such apparent differences in average RET values among these

270   taxa cannot be taken at face value and must be interpreted with great care, given the

271   small samples available for most of the taxa and the variation displayed by extant

272   taxa—as further illustrated by the range of *H. laietanus* (10.3–19.1, N=17), which

273   broadly overlaps the values for the remaining taxa. Our results for average 3D RET

274   (Table 2, Fig. 1B; see Fortuny *et al*. 2020, table 5 and fig. 7B) also indicate that *D.*

275   *fontani* (11.9) and "*S.*" *occidentalis* (19.0) display the thinnest and thickest enamel,

276 respectively, with the remaining taxa showing intermediate average values; in order of

277 increasing 3D RET: *H. crusafonti* (12.1), *A. brevirostris* (12.9), *H. laietanus* (13.5),

278 and *P. catalaunicus* (15.5). Although the "*S.*" *occidentalis* sample displays the thickest

279 enamel, it should be taken into account that this result is likely biased by small size

280 coupled with the lack of first molars available for analysis.

281   Statistical comparisons based on Kruskal-Wallis tests for equality of medians show

282 significant differences among extant apes in both 2D RET ($\chi^2 = 38.31$, $p < 0.001$) and

283 3D RET ($\chi^2 = 32.05$, $p < 0.001$). Mann-Whitney pairwise comparisons in 2D and 3D

284 RET (See Fortuny *et al*. 2020, table 6) indicate that African apes (*Gorilla* and *Pan*)

285 and siamangs display similarly thin enamel, whereas orangutans and gibbons display

286 significantly thicker enamel (see average and maximum-minimum values in Fortuny *et*

287 *al*. 2020, tables 7 and 8). Chimpanzees display slightly thicker enamel than gorillas

288 only for 3D RET, whereas differences in 2D RET become nonsignificant after

289 Bonferroni correction, and the same occurs between siamangs and gibbons.

290   Comparisons between the fossil samples and extant taxa are possible for both 2D

291 and 3D RET (Fortuny *et al*. 2020, tables 7 and 8, respectively), but comparisons with

292 other extinct taxa are mostly restricted to 2D RET due to the lack of 3D data (with

293 only two exceptions; see Fortuny *et al*. 2020, table 8). We therefore compared 2D

294 RET among Iberian dryopithecines, extant hominoids, and two fossil hominoid

295 samples—the kenyapithecine *Griphopithecus* and the dryopithecine *Rudapithecus* (see

296 descriptive statistics in Fortuny *et al*. 2020, table 9 and fig. 7A)—whereas

297 comparisons for 3D RET were restricted to Iberian dryopithecines and extant taxa (see

298 Fortuny *et al*. 2020, table 10 and fig. 7B).

299   When these enlarged samples are considered, Kruskal-Wallis tests show again

300 significant differences in both 2D RET ($\chi^2 = 23.44$, $p < 0.001$) and 3D RET ($\chi^2 =$

301   13.84, p < 0.001). Mann-Whitney pairwise comparisons are reported for fossil taxa as

302   compared with the extant hominoid samples discussed above (see Fortuny *et al*. 2020,

303   table 11). Based on the currently available, restricted fossil samples, 2D RET

304   comparisons indicate that all extinct taxa show thicker enamel than gorillas and

305   chimpanzees, and most also display thicker enamel than siamangs, with the exception

306   of *D. fontani* (although differences also approach the 0.05 significance threshold, for

307   *H. laietanus* and *Rudapithecus*). In contrast, most extinct taxa display lower 2D RET

308   than *Pongo*, except *Griphopithecus*, *P. catalaunicus* and "*S.*" *occidentalis*, which do

309   not differ from orangutans. However, like most other extinct taxa, *P. catalaunicus*

310   does not differ from gibbons, whereas *Griphopithecus* and "*S.*" *occidentalis* show

311   instead thicker enamel (although the "*S.*" *occidentalis* sample is biased, as explained

312   above) (Fortuny *et al*. 2020, fig. 7A).

313   Based on 3D RET, less significant differences are found, probably as a result of

314   smaller sample sizes. Only "*S.*" *occidentalis* clearly shows thicker enamel than extant

315   apes (although this is probably biased, see above), whereas *H. laietanus* and *A.*

316   *brevirostris* display thicker enamel than siamangs and gorillas (although comparisons

317   with chimpanzees only approach significance), while *P. catalaunicus* further displays

318   thicker enamel than chimps, more closely resembling orangs and gibbons.

319   Adjusted z-scores for 2D RET (see Fortuny *et al*. 2020, fig. 8A, table 12) and 3D

320   RET (see Fortuny *et al*. 2020, fig. 8B and table 13) for each fossil specimen compared

321   with extant hominoid samples may clarify the results provided above, especially for

322   the smaller samples, as it is the case for "*S.*" *occidentalis* in both 2D RET and 3D

323   RET, as well as *P. catalaunicus*, *H. crusafonti*, and *D. fontani* in 3D RET. Due to the

324   extensive overlap among extant taxa, particularly when all tooth loci are considered

325   simultaneously, many specimens fit within the variation of all the comparative

326   samples, although others do significantly differ from some. For all the taxa examined,

327   some specimens differ from African apes and, for *H. laietanus*, *P. catalaunicus*, and

328   "*S.*" *occidentalis*, also from siamangs, whereas most specimens do not differ from

329   either gibbons or orangutans. In fact, in 2D only a single specimen of *H. laietanus* and

330   two of "*S.*" *occidentalis* show significantly thicker enamel than orangutans, whereas in

331   3D there is a single specimen of "*S.*" *occidentalis* that shows thicker enamel than both

332   siamangs and humans. While the Miocene ape's sample size available for 3D

333   estimates is smaller than for 2D analyses, the results show high coherence.

334

335   *Enamel distribution maps*

336   Enamel distribution maps (Figs 2 and 3) in *D. fontani* upper molars show that the

337   thickest enamel is on the periphery of the cusps and marginal ridges, with much

338   thinner enamel in the trigon than over the talon basin. The upper molars of *P.*

339   *catalaunicus*, *A. brevirostris* and *H. laietanus* overall show a similar enamel

340   distribution pattern to *D. fontani*, except that the enamel is relatively thicker on the

341   trigon basin. A specimen of *H. laietanus* (IPS58340) somewhat differs by having its

342   thickest enamel limited for the most part to the protocone, while both the trigon and

343   talon basins display thinner enamel. In the upper molars of *H. crusafonti*, thicker

344   enamel is distributed over the talon basin and lateral walls, although, with the

345   exception of the protocone, the trigon enamel is moderately thin to thin. In the lower

346   molars of *H. laietanus*, the thickest enamel is found on the periphery of the talonid,

347   while the trigonid (even buccally) generally shows moderately thick enamel. The only

348   exception is IPS1822 (the invalid holotype of *"D. piveteaui"*, currently included in *H.*

349   *laietanus*), which displays its thickest enamel only on the outer aspect of the buccal

350   cusps, as in the paratype of *H. crusafonti* IPS1816. The molars of *H. crusafonti*

14

351   MGSB25314 have in contrast their thickest enamel located on the outer aspect of the

352   cusps, their inner aspects being also relatively thick (only the center of the occlusal

353   basin and the cervical part of the crown are thin enameled). The holotype of "*S.*"

354   *occidentalis*, in turn, displays a similar enamel distribution pattern as IPS1822 and

355   IPS1816, with the thickest areas mostly located on the buccal half of the crown

356   (notably on the outer aspect of the buccal cusps, up to the cusp apex), and thinner

357   enamel being located lingually. "*Sivapithecus*" *occidentalis* IPS41734, although

358   somewhat worn, also approximates the enamel distribution shown by IPS1822 and the

359   holotype of "*S.*" *occidentalis*.

360

361   *EDJ morphology*

362   Outer enamel surface morphology (see Fortuny *et al*. (2020, figs 9 and 10) of all the

363   dryopithecine upper molars considered in this study displays a similar pattern, which

364   is also reflected at the EDJ but with a sharper topography (Fig. 4; Table 3). All the

365   M^1s and M^2s display four developed dentine horns at the EDJ, corresponding to the

366   four main cusps visible on the OES (see Fortuny *et al*. 2020, fig. 9), whereas in the M^3

367   one of the two distal cusps is frequently absent in accordance with their generally

368   shorter and more distally-tapering crowns. Thus, no hypocone dentine horn is

369   expressed in the M^3 of *P. catalaunicus* (Fig. 4C), whereas it is well expressed *A.*

370   *brevirostris* (Fig. 4J) and *H. crusafonti* (Fig. 4T,U), and discernible (even if smaller)

371   in *D. fontani* (Fig. 4G). In the M^3 of *H. laietanus*, the hypocone is present, but the

372   metacone horn is very poorly developed (Fig. 4X,Y), which contrasts with the distinct

373   M^3 metacone displayed by the other taxa (with the exception of one M^3 of *H.*

374   *crusafonti*; Fig. 4T). The dentine horns of the upper molar four main cusps are more

375   centrally situated in *P. catalaunicus* and especially in *D. fontani* (Fig. 4D–G) than in

376   *A. brevirostris, H. crusafonti* and especially *H. laietanus* (Fig. 4V–Y), which have

377   more peripheral and vertically set dentine horns, in accordance with their less flaring

378   crowns. In the M^1s and M^2s of *A. brevirostris* (Fig. 4H,I,M–P) and *H. crusafonti* (Fig.

379   4Q–S), the hypocone dentine horn is clearly more lingual than the protocone, as in the

380   *D. fontani* M^1 (Fig. 4E) but unlike in the remaining specimens.

381   The mesial fovea, slit-like at the OES, appears as a larger, ovoid to subrectangular

382   depression at EDJ level, even if much smaller than the trigon basin, particularly in the

383   M^3s. This fovea appears shallower and slightly more inclined mesialward in *P.*

384   *catalaunicus* (Fig. 4A–C) and *D. fontani* (Fig. 4D–G) than in the remaining species,

385   and also more mesially projected in the latter. In *A. brevirostris* (Fig. 4H–P) and

386   especially *Hispanopithecus* spp. (Fig. 4Q–Y), the mesial fovea is mesiodistally

387   shorter, more buccally positioned, deeper, and enclosed by a stronger mesial marginal

388   ridge. The mesial fovea is generally separated from the trigon basin by a well-

389   developed hypoparacrista that links the paracone with the protoconule (except in a few

390   specimens, e.g., Fig.4U,V). The protoconule is often obliterated by wear on the OES,

391   but a distinct dentine horn subequal in size to those of the four main cusps is

392   frequently evidenced at the EDJ, even if variably developed: it is generally less

393   developed in M^3 (except in *P. catalaunicus*; Fig. 4C), and only poorly developed in

394   the M^2 of *D. fontani* MGSB48486 (Fig. 4D). The hypoparacrista generally terminates

395   at the protoconule, but in some instances it joins the mesial marginal ridge, as in the

396   M^3s of *P. catalaunicus*, *D. fontani*, *A. brevirostris* and *H. crusafonti* (Fig. 4C,G,J,T),

397   and some M^2s of *A. brevirostris* (Fig. 4L) and *H. laietanus* (Fig. 4W). In the two latter

398   taxa, a secondary small dentine horn is also present at the junction of the

399   hypoparacrista with the marginal ridge. The hypoparacrista generally originates nearby

16

400   the paracone dentine horn apex, although in the M^3 of *D. fontani* and *A. brevirostris*

401   (Fig. 4G,J) it originates more mesially.

402   At the EDJ, the trigon basin displays a subrhomboid contour (instead of a triangular

403   one, as in the OES) in all the taxa, but is shallower in *D. fontani* (Fig. 4D–G) and *H.*

404   *laietanus* (Fig. 4V–Y). The crista obliqua is high, complete and generally straight in *P.*

405   *catalaunicus* (Fig. 4A–C) and *A. brevirostris* (Fig. 4H–M), although it is somewhat

406   discontinuous (Fig. 4N–O) or even poorly developed (Fig. 4P) is some molars of the

407   latter species. In *D. fontani* (Fig. 4D–G), the crista obliqua is low and less straight, due

408   to the slightly curved postprotocrista, resulting in a sinuous crista obliqua in one

409   specimen (Fig. 4G). In *Hispanopithecus* spp. (Fig. 4Q–Y), the crista obliqua is even

410   lower and more diffuse, particularly in *H. crusafonti* (Fig. 4Q–U), being interrupted

411   (non-merging postprotocrista and hypometacrista) in the two M^{3}s of *H. crusafonti*

412   (Fig. 4T,U) and one of the M^{3}s of *H. laietanus* (Fig. 4X). In all the taxa, the talon

413   basin is subtriangular and smaller than the trigon basin, also being shallower than the

414   latter in *P. catalaunicus* (Fig. 4A–C), *A. brevirostris* (Fig. 4H–P) and *H. crusafonti*

415   (Fig. 4Q–U). In most specimens, the talon basin is divided by a transverse and low

416   hypocone-metacone crista, more clearly discerned at the EDJ than at the OES. This

417   crista is generally more distinct in the M^1 than in the M^2, and absent from the M^3.

418   When present, it delimits a distal fovea from the deeper and more expansive talon

419   basin, originating from the hypocone dentine horn and joining the end of the

420   postmetacrista (only with some exceptions; Fig. 4K,Q,V).

421   The upper molars display a subquadrangular (M^1) to subrectangular (M^2) occlusal

422   outline, except for the M^3 of *P. catalaunicus*, *A. brevirostris* and *H. laietanus* (Fig.

423   4C,J,X,Y), which display an ovoid to subtriangular profile due to the truncated talon.

424   The degree of talon development is quite variable in *Hispanopithecus*, as previously

17

425 noted based on the OES (Alba *et al.* 2012*b*), encompassing differences among the

426 other species in this regard. The degree of buccolingual waisting of the upper molars

427 at EDJ level is more marked in *A. brevirostris* (Fig. 4H,I,K–P), slightly less developed

428 in *D. fontani* (Fig. 4D–G), more variable in *H. crusafonti* and *H. laietanus* (Fig. 4Q–

429 W), and least developed in *P. catalaunicus* (Fig. 4A,B). The weak to moderate

430 development of the lingual cingulum at the OES is variably expressed at the EDJ,

431 ranging from the lack of this feature to a shelf bordered by a (semi)continuous crest

432 extending along the lingual aspect of the protocone, sometimes connecting the lingual

433 groove separating the protocone and hypocone. Even if decreasing in expression from

434 the M^1 to the M^3, the lingual cingulum tends to be more developed in *A. brevirostris*

435 and *H. crusafonti* (Fig. 4H–U), only moderately expressed in *D. fontani* (Fig. 4D–G),

436 and even less so in *P. catalaunicus* (Fig. 4A, B,C) and *H. laietanus* (Fig. 4V,W). A

437 buccal cingular remnant (in the form of a short crest enclosing a small fovea)

438 frequently appears at the external end of the buccal groove at the EDJ in the M^1 and

439 most M^2 of *A. brevirostris* (Fig. 4H,K,L–P) and *H. crusafonti* (Fig. 4Q–S). Similarly, a

440 shelf-like structure is visible at the same spot in some specimens of *D. fontani* (Fig.

441 4E,F) and the M^1 of *P. catalaunicus* (Fig. 4A). In contrast, the buccal aspect is rather

442 smooth in *H. laietanus* (Fig. 4V,W) and the remaining specimens of *P. catalaunicus*

443 (Fig. 4B).

444   The overall endostructural pattern of the lower molars (Fig. 5; Table 4) is similar to

445 the OES morphology (see Fortuny *et al*. 2020, fig. 10), with five well-developed

446 dentine horns corresponding to the five main cusps. The dentine horns are generally

447 vertically set, with the exception of the metaconid dentine horn of "*S.*" *occidentalis*

448 specimens (Fig. 5A–C), which is tilted toward the center of the tooth. In some

449 specimens of *Hispanopithecus* spp., the metaconid dentine horn is also somewhat

450   centrally tilted (especially in the M$_3$ of MGSB25314; Fig. 5J), although to a lesser

451   extent. The lingual dentine horns are very peripherally situated relative to the crown

452   margin, whereas those corresponding to protoconid and hypoconid are less peripheral.

453   This is more clear-cut in "*S.*" *occidentalis* specimens (Fig. 5A–C) compared to

454   *Hispanopithecus*, although this feature is variable within both *H. crusafonti* (Fig. 5G–

455   J) and *H. laietanus* (Fig. 5K–S). At the OES, *H. laietanus* (see Fortuny *et al*. 2020,

456   fig.10K, N–S) displays a more reduced buccal cingulid than the remaining taxa (see

457   Fortuny *et al*. 2020, fig. 10A–J), in which it is nevertheless discontinuous. This

458   difference is more marked at the EDJ (Fig. 5), where the buccal cingulid becomes

459   shelft-like (at least between protoconid-hypoconid and hypoconid-hypoconulid)

460   except in *H. laietanus* (Fig. 5K, N–S), in which it is only minimally developed if at all.

461   Buccolingual crown waisting is also more strongly expressed at the EDJ, being most

462   marked in *H. laietanus* (Fig. 5K, N–S) both buccally and lingually, whereas in "*S.*"

463   *occidentalis* (Fig. 5A–C) as well as in *H. crusafonti* (Fig. 5G–J) waisting is moderate

464   to slight.

465   Some specimens express additional cuspulids at the EDJ level. While no

466   tuberculum sextum (C6) is expressed in any specimen at either the OES or the EDJ

467   levels, the M$_2$ of "*S.*" *occidentalis* holotype (Fig. 5B) and an M$_2$ of *H. crusafonti* (Fig.

468   5G) display a well-developed interconulid-type tuberculum intermedium (C7) at the

469   distal end of the postmetacristid, which at the OES is merely expressed as a secondary

470   (cuspulid-like) thickening of the enamel. Furthermore, the M$_2$ of "*S.*" *occidentalis*

471   specimens (Fig. 5A–C) display a mesiodistally-elongated metaconid dentine horn with

472   a distinct tuberculum intermedium or metaconulid-type C7 horn just distally from the

473   main metaconid dentine horn. This 'twinned' metaconid morphology, also expressed

474   at the OES as a cuspulid-like enamel thickening, is lacking in *H. crusafonti* (Fig. 5G–

475   J), but variably expressed (although to a lesser extent) in most lower molars of *H.*

476   *laietanus* (Fig. 5K, N–S), sometimes being discernible at the OES (see Fortuny *et al*.

477   2020, fig. 10K,L,N,O,R).

478   The mesial fovea is much shorter mesiodistally than buccolingually broad and not

479   completely isolated from the much deeper and more extensive talonid basin, since the

480   hypoprotocristid and hypometacristid junction is interrupted by a mesiodistal fissure.

481   These cristids, less discernible at the EDJ than the OES, are less marked in

482   *Hispanopithecus* spp. (Fig. 5G–S) than the remaining taxa (Fig. 5A–C). At the EDJ,

483   the cristid obliqua generally appears more distinct than at the OES, although it is also

484   incomplete (the postprotocristid and prehypocristid junction is interrupted, although

485   the buccolingual groove present at the OES is not discernible at the EDJ). Similarly,

486   the profuse development of secondary enamel wrinkling on the talonid basin displayed

487   by some specimens ("*S.*" *occidentalis* and *H. laietanus*; see Fortuny *et al*. 2020, fig.

488   10B,C,S) has no concomitant expression at the EDJ. Only the obliquely-oriented crest

489   (postcristid + hypoentocristid) separating the talonid basin from the more restricted

490   distal fovea at the OES of most specimens (even if partially interrupted by a

491   mesiodistal groove; see Fortuny *et al*. 2020, fig. 10) can generally be discerned at the

492   EDJ. However, on the latter it is variably expressed, ranging from a continuous but

493   low crest in most specimens, to a poorly expressed or even indistinguishable structure

494   in some M$_2$s (Fig. 5I,O,Q) and M$_3$s (Fig. 5C,R,S).

495

496   **DISCUSSION**

497   Our results allow us to refine these previously-reported differences in RET and

498   dental morphology among middle Miocene hominoids from Catalonia (Alba & Moyà-

499   Solà 2012; Alba *et al*. 2010*b*, 2013, 2020; Pérez de los Ríos *et al.* 2013) and further

500   provide additional information regarding the distinction between the late Miocene

501   species *H. laietanus* and *H. crusafonti* (Begun 1992; Cameron 1999; Alba *et al.*

502   2012*b*).

503

504   *Enamel thickness*

505   This study extends the previously published results of 2D RET for middle Miocene

506   dryopithecines from Catalonia (Alba *et al.* 2013, 2020) to *Hispanopithecus*—for

507   which only limited evidence was available in the case of *H. laietanus*, based on a few

508   histological sections (Andrews & Martin 1991; Kelley *et al.* 2001; Smith *et al.* 2019).

509   Most importantly, however, we first report 3D RET results for all these taxa. The

510   enamel of *A. brevirostris* was originally reported as similarly thick to that of *P.*

511   *catalaunicus* (Moyà-Solà *et al.* 2009*b*; Alba *et al.* 2010*b*), and both were assessed as

512   considerably thicker-enameled than *D. fontani* (Alba *et al.* 2010*b*), thereby

513   contradicting the previous contention that all the middle Miocene dryopithecines from

514   Catalonia were thin-enameled (Begun 2009) as well as the purported synonymy of the

515   former with *D. fontani* (Begun 2007, 2009). Later on, the significance of such

516   differences was disputed on the basis that enamel thickness is too variable among

517   extant and extinct hominoids to be reliable as a taxonomic criterion (Begun *et al.*

518   2012). Such differences were subsequently confirmed to some extent using slightly

519   enlarged samples for *A. brevirostris* and *D. fontani* and based on higher resolution

520   scans (the same used in this paper; Alba *et al.* 2013, 2020). However, the latter studies

521   showed that both *A. brevirostris* and *P. catalaunicus* display thinner enamel than

522   originally reported (Alba *et al.* 2010*b*), being more similar to extant orangutans, albeit

523   still significantly thicker than *D. fontani*, most similar to extant African apes (Alba *et*

524   *al.* 2013, 2020).

525   Caution is required when interpreting the RET values, given the small samples

526   analyzed for most extinct taxa, which preclude analyzing sexes or dental loci

527   separately, given the confounding effects of both sexual dimorphism (lower 2D RET

528   values in males) and tooth position (2D RET increase from first to third molars; Smith

529   *et al.* 2005, 2012*b*, 2019). This is highlighted by the 2D RET results newly reported

530   here for *H. crusafonti* and especially *H. laietanus*, since the comparatively larger

531   sample for the latter species shows a wide range of variation (10.3–19.1; Table 2, see

532   Fortuny *et al*. 2020, fig. 6) that almost encompasses all the remaining taxa. Similarly,

533   all the extant taxa represented by adequate samples display a wide range of variation

534   in 2D and 3D RET (with maximum values often almost doubling minimum values).

535   Sexual dimorphism might play some role in this regard, given that Smith *et al.*

536   (2012*b*) found higher 2D RET values for male than for female orangutans, although

537   differences were not significant for molar loci except in the M^3, and differences

538   between tooth loci appear larger. All these factors cannot be adequately addressed in

539   the studied samples, indicating that caution is warranted for extinct taxa represented

540   by small samples. Among hominoids from Catalonia, only *H. laietanus* (N=17) is well

541   represented, although the samples of *P. catalaunicus* (N=5), *A. brevirostris* (N=9) and

542   *H. crusafonti* (N=7) are still greater than for most other extinct apes except for

543   *Griphopithecus* (N=8), *Rudapithecus hungaricus* (N=8) and *Gigantopithecus blacki*

544   (N=7).

545   While 3D RET is useful for comparing the Iberian dryopithecines with one another

546   and with extant hominoids, comparisons with most extinct hominoids are generally

547   limited to 2D RET data (Smith *et al.* 2019). This is problematic because, even though

548   2D and 3D RET results are generally in good agreement, this is not always the case

549   due to differences in enamel distribution throughout the crown, as illustrated by the

550   cartographies shown in Figures 2 and 3. Interestingly, the range of 3D RET for *H.*

551   *laietanus* (10.5–16.4; Table 2) is less extensive than for 2D RET. Furthermore, 3D

552   RET results are arguably more informative because they reflect the global pattern of

553   enamel distribution.

554   Taken together, the data reported here both in 2D and 3D support the view that

555   Iberian dryopithecines, like *Rudapithecus* from Hungary and *Danuvius* from Germany

556   (see below), are thicker-enameled than African apes (especially gorillas), and most

557   similar to the condition displayed by extant gibbons and, to a lesser extent,

558   orangutans—with the exception of "*S.*" *occidentalis* (which clearly displays thicker

559   enamel, most similar to *Griphopithecus*) and also *P. catalaunicus* (which more closely

560   approaches the orangutan condition, particularly in 3D). The 2D RET for

561   *Rudapithecus* (14.35, range 11.29–17.48, N=8; Smith *et al.* 2019) fits well with the

562   ranges reported for most Iberian dryopithecines except "*S.*" *occidentalis* (and

563   particularly with the variation displayed by *H. laietanus*), whereas *Danuvius* (16.03,

564   N=1; Böhme *et al.* 2019) appears most similar to *P. catalaunicus* based on the single

565   reported figure for this taxon (a second molar). There is the possibility that *D. fontani*

566   and *H. crusafonti* display thinner enamel than the remaining taxa (including *A.*

567   *brevirostris* and *H. laietanus*), apparently being more similar to chimpanzees, but this

568   cannot be demonstrated based on the small available samples available for these taxa.

569   Assuming that "*S.*" *occidentalis* likely belongs to one of the taxa recorded at ACM

570   other than *D. fontani* (Alba *et al.* 2020), our RET results tentatively support its

571   synonymy with *P. catalaunicus*. As already explained, the RET figures for "*S.*"

572   *occidentalis* are probably exaggerated because there is no first molar available, so that

573   combining with sample with *P. catalaunicus* would result in a taxon with an enamel

574   thickness most similar to orangutans. In contrast, combining the "*S.*" *occidentalis*

575 sample with that of *A. brevirostris* would result in an even wider range of variation

576 than that documented for *H. laietanus*.

577 Hominoids as a whole are generally thicker-enameled than other anthropoids

578 (Olejniczak *et al.* 2008*a*), although displaying considerable interspecific variation

579 (Martin 1985; Schwartz 2000; Smith *et al.* 2005, 2008; Olejniczak *et al.* 2008*a*).

580 Enamel thickness is labile on evolutionary terms due to convergent and relatively

581 rapid dietary adaptations (Andrews & Martin 1991; Alba *et al.* 2010*b*). Thick enamel,

582 in particular, has been classically linked to sclerocarpy—i.e., the consumption of hard-

583 foot items (Martin 1985; Andrews & Martin 1991; Vogel *et al.* 2008). This has been

584 related to selection pressures for low cusp relief and reduced hearing crests (Andrews

585 & Martin 1991) or the biomechanical need to prevent the propagation of radial cracks

586 from the EDJ during the mastication of hard foods (Vogel *et al.* 2008). However,

587 although there seems to be some general correspondence between the overall

588 properties of the food habitually consumed and tooth structure in primates, linking

589 enamel thickness with specific diets is not necessarily, especially in instances where

590 phylogenetically closely-related species that consume different kinds of food are

591 considered (Grine and Daegling, 2017). Our 2D RET results suggest that most of the

592 Iberian Miocene dryopithecines present thicker enamel than African apes (especially

593 gorillas) and in some cases also than siamangs, which display folivorous tendencies

594 despite a mainly frugivorous diet. In contrast, RET results from Iberian fossil

595 dryopithecines are virtually identical to gibbons, and apparently somewhat lower than

596 in orangutans. This agrees with a soft frugivorous diet for Iberian dryopithecines, with

597 the exception of *Pierolapithecus*. The latter more closely resembles orangutans, which

598 unlike gibbons displays a scleroparpic component in its diet. This is consistent with

599 microwear data suggesting a frugivorous diet with an orang-like, arboreal hard-object

600   component for *Pierolapithecus* (DeMiguel *et al.* 2014), but lacking a specialized hard-

601   object diet as that inferred for *Griphopithecus*.

602   The hypothesis that thick enamel and other dentognathic adaptations to sclerocarpic

603   feeding were the key adaptation that facilitated the dispersal of hominoids out of

604   Africa into Eurasia (Begun 2003) was favored based on previous data (Alba *et al.*

605   2010*b*) indicating that both *Pierolapithecus* and *Anoiapithecus* were as thick-enameled

606   as earlier African afropithecids (*Afropithecus*), Eurasian putative stem hominids

607   (*Griphopithecus*), and early pongines from Asia (*Sivapithecus*). Our results do not

608   disprove this view, based on the earliest Eurasian forms (*Griphopithecus*), but indicate

609   that it cannot be supported further based on Iberian dryopithecines, which display an

610   enamel thickness and microwear signal overall more in agreement with soft frugivory

611   (Alba *et al.* 2010*b*; DeMiguel *et al.* 2014). Whether the apparently thicker-enameled

612   *Pierolapithecus* (particularly if "*S.*" *occidentalis* belongs to the same taxon) retains the

613   plesiomorphic condition or represents a secondary reversal among the dryopithecine

614   radiation cannot be determined.

615

616   *Enamel distribution maps*

617   Enamel distribution maps further enable a more refined assessment of enamel

618   thickness, as it has been shown that molar enamel thickness distribution may differ

619   between taxa with close 3D RET values, indicating that the latter might not adequately

620   reflect molar functional and/or taxonomic signals (Kono 2004; Kono & Suwa 2008;

621   Macchiarelli *et al.* 2008, 2009; Olejniczak *et al.* 2008*b*,*c*; Suwa & Kono 2005; Suwa

622   *et al.* 2009). Enamel distribution maps of the upper molars of Miocene dryopithecines

623   from Catalonia show that *P. catalaunicus*, *A. brevirostris*, *D. fontani* and *H. laietanus*

624   exhibit a similar pattern, with the thickest enamel lying over the talon and lateral cusp

625   walls, and the trigon basin being considerably thinner (in *D. fontani*) to moderately

626   thinner (in the other taxa). In this regard, dryopithecines differ from extant apes, with

627   *Pan* and *Hylobates* exhibiting their thickest enamel peripherally (on the external

628   aspect of the cusps) and much thinner occlusal enamel, and *Gorilla* and *Pongo*

629   approximating this pattern but displaying relatively thicker occlusal enamel (Kono

630   2004; Kono & Suwa 2008; Suwa *et al.* 2009).

631   While enamel distribution in the upper molars does not differ among the

632   investigated taxa, for the lower molars it shows differences between *H. laietanus* and

633   *H. crusafonti*. The distinction between these species and the inclusion of the mandible

634   MGSB25314 in *H. crusafonti* instead of *D. fontani* has been supported by some

635   authors (Begun 1992, 2002; Alba 2012; Alba *et al.* 2012*b*, 2013) but questioned by

636   others (Harrison 1991; Golpe Posse 1993; Ribot *et al.* 1996). The only examined

637   lower molar of *H. crusafonti* from its type locality differs from most specimens of *H.*

638   *laietanus* by displaying the thickest enamel on the buccal aspect of the buccal cusps

639   instead of the periphery of the whole talonid, thereby supporting their distinction. The

640   molars from the mandible MGSB25314 also differ from those of *H. laietanus*.

641   Nevertheless, they differ in a different way than the aforementioned paratype of *H.*

642   *crusafonti*, by displaying the thickest enamel on the external aspect of all cusps. This

643   is consistent with assignment of MGSB25314 to a species other than *H. laietanus*, but

644   it does not particularly supporting its assignment to *H. crusafonti*. The taxonomic

645   implications of these comparisons must remain tentative given the small sample of

646   lower molars available for *H. crusafonti* from the type locality, the lack of enamel

647   distribution maps for mandibular specimens of *D. fontani* from its type locality (Saint-

648   Gaudens, France), and the fact that a particular specimen of *H. laietanus* (the invalid

649 holotype of *Dryopithecus piveteaui* nomen nudum) more closely resembles the single

650 examined paratype of *H. crusafonti*.

651   In turn, the enamel distribution of "*S.*" *occidentalis* specimens, characterized by the

652 presence of thicker areas mostly on the buccal half of the crown and thinner lingual

653 enamel further supports their attribution to a single taxon. However, the restricted

654 sample sizes available—in particular, the lack of lower molar distribution maps for

655 both other middle Miocene dryopithecines (particularly *P. catalaunicus* and *A.*

656 *brevirostris*, which might be conspecific with the former; Alba *et al.* 2020)—and

657 further similarities with some specimens of *Hispanopithecus* (especially IPS1822)

658 preclude a conclusive assessment of the taxonomic implications of enamel

659 distribution.

660

661 *EDJ morphology*

662   Contrasting with the traditional emphasis on OES for assessing dental morphology,

663 the usefulness of the EDJ has been recently stressed (Olejniczak *et al.* 2004; Skinner

664 2008; Skinner *et al.* 2008*a*, 2009*b*, Skinner *et al.* 2008b, 2009a; Zanolli *et al.* 2012,

665 2014; Zanolli & Mazurier 2013; Davies *et al.* 2019; Détroit *et al.* 2019), given that it

666 provides highly-diagnostic additional information for taxonomic identification (Smith

667 *et al.* 2006; Skinner *et al.* 2008*a*, 2008*b*, 2009, Zanolli *et al.* 2012, 2014, 2019); and

668 enables tooth morphology comparisons irrespective of occlusal wear (Tables 3 and 4).

669 The thicker and more inflated crests, secondary enamel folds, and cusp bases that

670 distinguish *P. catalaunicus* from *A. brevisrostris* and *D. fontani* at the OES (Alba *et*

671 *al.* 2013; Pérez de los Ríos *et al.* 2013) are not reflected at the EDJ, thus being

672 probably attributable to the overall thicker enamel of the former. However, *P.*

673 *catalaunicus* also differs from these genera in other upper molar features observable at

674   the EDJ: from *D. fontani*, in the deeper trigon basin, the higher and straighter crista

675   obliqua, the M^1 hypocone dentine horn more aligned with that of the protocone (in

676   agreement with OES morphology; Alba *et al.* 2013; Pérez de los Ríos *et al.* 2013), the

677   less buccolingually waisted upper molars, and the less developed lingual cingulum;

678   and from *A. brevirostris*, in the shallower and less restricted mesial fovea, the M^1 and

679   M^2 hypocone horn less lingually situated relative to that of the protocone (in

680   agreement with the OES morphology; Alba *et al.* 2013; Pérez de los Ríos *et al.* 2013),

681   the markedly less buccolingually waisted upper molars, and the much less developed

682   lingual cingulum.

683   As previously reported (Alba *et al.* 2020), the EDJ morphology of the ACM/BCV4

684   specimen supports its conspecificity with the holotype of "*S.*" *occidentalis*, only

685   differing in the lack of a tuberculum intermedium in the former—which is variable in

686   *H. crusafonti* and hence likely atributable to intraspecific variation. These similarities

687   (and those in enamel thickness and distribution mentioned above) strengthen the

688   attribution of the ACM/BCV4 specimen to the same taxon as the holotype of "*S.*"

689   *occidentalis* (Alba *et al.* 2020). The latter specimen (originally consisting of a

690   mandibular fragment, but currently preserved as isolated M_2 and M_3; Golpe Posse

691   1993) was initially assigned to *D. fontani* (Villalta Comella & Crusafont Pairó, 1941)

692   but soon thereafter used to erect a new species (Villalta Comella & Crusafont Pairó,

693   1944). Over the years, "*S.*" *occidentalis* has been mostly synonimized with

694   *Hispanopithecus laietanus* (or *Dryopithecus laietanus*) (Crusafont Pairó & Hürzeler

695   1961; Simons & Pilbeam 1965; Begun *et al.* 1990; Harrison 1991; Golpe Posse 1993;

696   Ribot *et al.* 1996), later considered a nomen dubium (Moyà-Solà *et al.* 2004, 2009*a*;

697   Casanovas-Vilar *et al.* 2011; Alba 2012; Marigó *et al.* 2014; Alba *et al.* 2017) and

698   recently considered as species inquirenda (Alba *et al.* 2020). In particular, based on 2D

699 RET and both EDJ and OES similarities, it was recently concluded that "*S.*"

700 *occidentalis* is not synonymous with *D. fontani*, but given the lack of well-preserved

701 M$_2$ of *A. brevirostris* is was not possible to favor a synonymy with *P. catalaunicus*

702 over the latter species (Alba *et al.* 2020). The 3D RET results reported above

703 tentatively support the view that "*S.*" *occidentalis* represent the otherwise unknown

704 lower dentition of *P. catalaunicus*, in which case the former species epithet would take

705 priority. On the other hand, we consider it unadvisable to formally synonymize these

706 taxa until an alternate assignment to *A. brevirostris* can be more convincingly

707 excluded based on additional mandibular material unequivocally assignable to *P.*

708 *catalaunicus* (i.e., ideally associated with cranial remains).

709   The EDJ morphology is also informative regarding the alpha-taxonomy of

710 *Hispanopithecus*, which was erected with *H. laietanus* as its type species in 1944

711 (Villalta Comella & Crusafont Pairó 1944), but it was later synonymized with

712 *Dryopithecus* (Simons & Pilbeam 1965). For many years, such synonymy was

713 accepted by most authors (Begun *et al.* 1990; Harrison 1991; Begun 1992, 2002, 2007;

714 Moyà-Solà & Köhler 1993, 1995, Ribot *et al.* 1996; Andrews *et al.* 1996), with only a

715 few exceptions (Golpe Posse 1993; Cameron 1997, 1998, 1999). Indeed, *H. crusafonti*

716 was originally described within *Dryopithecus* (Begun 1992), but subsequently

717 reallocated to *Hispanopithecus* only by a few authors (e.g., Cameron 1999) until the

718 discovery of ACM dryopithecines permitted to re-establish the distinct generic status

719 of *Hispanopithecus* on a more firm basis (Moyà-Solà *et al.* 2009*a*; Begun 2009). This

720 has been subsequently accepted by most authors (Begun 2010, 2015; Moyà-Solà *et al.*

721 2009*b*; Casanovas-Vilar *et al.* 2011; Alba 2012; Alba *et al.* 2012*b*, 2013; Alba &

722 Moyà-Solà 2012; Begun *et al.* 2012; Pérez de los Ríos *et al.* 2013; Fleagle 2013;

723 Böhme *et al.* 2019), only with few exceptions (Pickford 2012) regarding *H. crusafonti*.

724   Our results show that the late Miocene *H. laietanus* and *H. crusafonti* differ from the

725   investigated middle Miocene taxa in the more peripheral dentine horns of the upper

726   molars (especially in *H. laietanus*) as well as in the lower and often disrupted crista

727   obliqua. They further differ from *P. catalaunicus* and *D. fontani*, but not *A.*

728   *brevirostris*, in the deeper and more restricted mesial fovea, and the somewhat more

729   marked buccolingual waisting of the upper molars (although this feature is variable).

730   All these features support the distinction of the genus *Hispanopithecus* from

731   *Dryopithecus* and other middle Miocene dryopithecine genera from the Vallès-

732   Penedès Basin.

733   It is noteworthy that the distinction of *H. crusafonti* from *H. laietanus* (Begun

734   1992, 2002, 2009; Cameron 1999; Moyà-Solà *et al.* 2009*a*; Casanovas-Vilar *et al.*

735   2011; Alba 2012; Alba & Moyà-Solà 2012; Alba *et al.* 2012*b*; Pickford 2012) was

736   questioned (Andrews *et al.* 1996) or even disputed (Harrison 1991; Ribot *et al.* 1996)

737   by some authors, who considered the former a junior subjective synonym of the latter.

738   The original diagnosis of *H. crusafonti* (Begun 1992) mentioned a series of differences

739   in tooth size and shape relative to *H. laietanus* that were later re-evaluated based on an

740   enlarged sample of upper teeth attributed to the latter species (Alba *et al.* 2012*b*). Such

741   re-evaluation concluded that incisor morphology and cheek teeth proportions

742   tentatively supported the distinction of two species, while the development of cingula

743   was too variable to serve as a taxonomically valid criterion. In fact, the original claim

744   that *H. crusafonti* displays more reduced cingula than *H. laietanus* (Begun 1992;

745   Cameron 1999) was already rejected based on the OES morphology (Ribot *et al.* 1996;

746   Alba *et al.* 2013). In turn, the presence of a more median hypocone and a better

747   developed metacone in the M^3 of *H. crusafonti* was considered potentially diagnostic,

748   although with doubts due to the small available samples and the high variability

749 displayed by the M^3 of *H. laietanus* (Alba *et al.* 2012*b*). Our assesment of the EDJ

750 morphology suggests that the two latter features are too variable to be diagnostic, but

751 leads us to identify alternative additional diagnostic features in the upper molars,

752 namely the more lingual position of the M^1 and M^2 hypocone, the less peripheral

753 dentine horns, the deeper trigon basin, and the more developed lingual cinglum in *H.*

754 *crusafonti*. It is particularly noteworthy that, at the EDJ, *H. crusafonti* displays better

755 developed cingula than *H. laietanus,* contrary to the conclusions in the original

756 description of the former species (Begun 1992), which relied on OES morphology.

757 Concerning the lower molars, several distinctive features noted in the original

758 description (deep and narrow grooves between the buccal cuspids or shallower and

759 more restricted talonid basins; Begun 1992) are not reflected in EDJ morphology. In

760 contrast, *H. crusafonti* (including the specimen MGSB25314) displays a more

761 developed buccal cingulid at the EDJ and less pronounced buccolingual waisting of

762 the lower molars than *H. laietanus*. Therefore, the EDJ evidence provided here for

763 both upper and lower molars, coupled with cheek tooth proportions and upper incisor

764 morphology (Alba *et al.* 2012*b*), support the distinction of the two *Hispanopithecus*

765 species. It should also be noted that, as previously noted for the OES (Alba *et al.*

766 2013), for some features (moderately peripheral upper molar dentine horns) *H.*

767 *crusafonti* more closely resembles the middle Miocene hominoids—especially *A.*

768 *brevirostris* (deeper trigon basin, lingually-positioned hypocone dentine horn, more

769 developed lingual cingulum)—than *H. laietanus* does. These features appear

770 plesiomorphic and might indicate a more basal position for *H. crusafonti*, although

771 additional (especially cranial) remains would be required to further test this

772 hypothesis.

31

773   Finally, although a single dryopithecine species is customarily recognized at Can

774   Llobateres (Begun *et al.* 1990, Harrison 1991; Begun 1992, 2002; Moyà-Solà &

775   Köhler 1993, 1995; Andrews *et al.* 1996; Ribot *et al.* 1996; Cameron 1997, 1999;

776   Casanovas-Vilar *et al.* 2011; Alba & Moyà-Solà 2012; Alba *et al.* 2012*b*), this is

777   worth revising in the light of the EDJ data reported here, particularly given previous

778   proposals that two additional species might be represented at this site (Crusafont Pairó

779   & Hürzeler 1961, 1969; Crusafont-Pairó & Golpe-Posse 1973): a smaller species

780   ("*Rahonapithecus sabadellensis*") and a larger one ("*Dryopithecus piveteaui*").

781   Although these species are nomenclaturally invalid (nomina nuda) (Simons & Pilbeam

782   1965; Begun *et al.* 1990; Alba & Moyà-Solà 2012; Alba *et al.* 2012*b*), some authors

783   have considered that the purported holotype of "*Rahonapithecus sabadellensis*"

784   (IPS1802, a mandibular fragment with M_1–M_3) might belong to the same taxon as the

785   holotype of "*S.*" *occidentalis* (Pickford 2012). Even if the M_3 of this specimen

786   displays the thickest value among the sample of this locality, this is not the case for 3D

787   RET, and overall the wide range of 2D RET values displayed by *H. laietanus* conform

788   to the levels of variation displayed by extant great ape species (see Fortuny *et al*. 2020,

789   table 7 and fig. 6). The lower molars from Can Llobateres 1, despite some variation in

790   EDJ morphology (e.g., in the presence of M_2 metaconulid), do not show marked

791   differences that might justify the distinction of additional species and are characterized

792   by the same features (e.g., poorly developed buccal cingulid and marked buccolingual

793   waisting) that distinguish the holotype of *H. laietanus* from the remaining investigated

794   taxa. The same applies to the EDJ morphology of the purported holotype of "*D.*

795   *piveteaui*" (IPS1822, an M_3 germ). This specimen merely stands out by its marked

796   development of enamel wrinkling at the OES, which is not reflected in any

797 concomitant differences from other *H. laietanus* specimens at the EDJ and is likely

798 attributable to the lack of wear.

799

800 **CONCLUSIONS**

801 Our reassessment of Iberian dryopithecine palaeobiodiversity in the light of the

802 reported data on tooth endostructural morphology is consistent with the distinction of

803 four different genera and five species of Miocene dryopithecines in Catalonia—a

804 distinction originally based on cranial morphology and features at the OES. Our

805 conclusions therefore reinforce the view that neither *Pierolapithecus*, *Anoiapithecus* or

806 *Hispanopithecus* can be considered junior synonyms of *Dryopithecus*. This also holds

807 for "*S.*" *occidentalis*, which must remain a species inquirenda until additional lower

808 molars of *P. catalaunicus* or *A. brevirostris* enable further comparisons. Our results

809 also show that the two late Miocene species of dryopithecines from Catalonia

810 (included in *Hispanopithecus*) display several derived features as compared to the

811 middle Miocene taxa. However, *H. crusafonti* generally retains a more primitive

812 morphology than *H. laietanus* and is thus more similar to the middle Miocene genera.

813 In the future, other aspects of the internal structure of the post-canine teeth of

814 these Miocene hominids and other extinct apes from Europe will be investigated to

815 extract additional paleobiological information. In particular, analyses of root

816 morphology (e.g., Kupczik and Hublin, 2010; Kupczik *et al.* 2019; Moore *et al.* 2013,

817 2016; Pan *et al.* 2019) and the application of morphometric geometric techniques to

818 quantify the EDJ shape (e.g., Skinner *et al.* 2009b, 2016; Zanolli *et al.* 2018, 2019)

819 will further highlight the Miocene hominid diversity.

820 However, pending the recovery and analysis of additional craniodental remains

821 in Europe (such as those of *Danuvius*; Böhme *et al.* 2019), this study confirms the

822   need for such kind of 3D tooth endostructural analyses in studies aimed at assessing

823   the alpha-taxonomy of fossil apes, as noted by some previous studies (Zanolli *et al.*

824   2019). The application of these techniques to currently available isolated dentognathic

825   fragments from elsewhere in Europe might ultimately unveil further the previously

826   unrecognized palaeobiodiversity of Miocene apes in this continent.

827

838

839   **DATA ARCHIVING STATEMENT**

840

841   Data for this study are available in MorphoSource and the Dryad Digital Repository:

842   https://morphosource.org/MyProjects/Dashboard/dashboard/select_project_id/1160

843

844   https://datadryad.org/stash/share/EiJrlF8TAY9FmzkrKqbzIcaiXBO8BD-

845   b1BSPjduY8Eg

846

847 **REFERENCES**

848 ALBA, D.M. 2012. Fossil apes from the Vallès-Penedès Basin. *Evolutionary*

849 *Anthropology*, **21**, 254–269.

850 — and MOYÀ-SOLÀ, S. 2012. On the identity of a hominoid male upper canine from

851 the Vallès-Penedès Basin figured by Pickford. *Estudios Geológicos*, **68**, 149–

852 153.

853 — — CASANOVAS-VILAR, I., GALINDO, J., ROBLES, J.M., ROTGERS, C.,

854 FURIÓ, M., ANGELONE, C., KÖHLER, M., GARCÉS, M., CABRERA, L.,

855 ALMÉCIJA, S. and OBRADÓ, P. 2006. Los vertebrados fósiles del Abocador

856 de Can Mata (els Hostalets de Pierola, l'Anoia, Cataluña), una sucesión de

857 localidades del Aragoniense superior (MN6 y MN7+8) de la cuenca del Vallès-

858 Penedès. Campañas 2002–2003, 2004 y 2005. *Estudios Geológicos*, **62**, 295–

859 312.

860 — — MALGOSA, A., CASANOVAS-VILAR, I., ROBLES, J.M., ALMÉCIJA, S.,

861 GALINDO, J., ROTGERS, C. and BERTÓ MENGUAL, J.V. 2010*a*. A new

862 species of *Pliopithecus* Gervais, 1849 (Primates: Pliopithecidae) from the

863 Middle Miocene (MN8) of Abocador de Can Mata (els Hostalets de Pierola,

864 Catalonia, Spain). *American Journal of Physical Anthropology*, **141**, 52–75.

865 — FORTUNY, J. and MOYÀ-SOLÀ, S. 2010*b*. Enamel thickness in the Middle

866 Miocene great apes *Anoiapithecus*, *Pierolapithecus* and *Dryopithecus*.

867 *Proceedings of the Royal Society B*, **277**, 2237–2245.

868 — ALMÉCIJA, S., and MOYÀ-SOLÀ, S. 2010*c*. Locomotor inferences in

869 *Pierolapithecus* and *Hispanopithecus*: Reply to Deane and Begun (2008).

870 *Journal of Human Evolution*, **59**, 143–149.

35

871 — MOYÀ-SOLÀ, S., and ALMÉCIJA, S. 2011. A partial hominoid humerus from the

872   middle Miocene of Castell de Barberà (Vallès-Penedès Basin, Catalonia,

873   Spain). *American Journal of Physical Anthropology*, **144**, 365–381.

874 — — ROBLES, J.M., and GALINDO, J. 2012*a*. The oldest pliopithecid record in the

875   Iberian Peninsula based on new material from the Vallès-Penedès Basin.

876   *American Journal of Physical Anthropology,* **147**, 135–140.

877 — CASANOVAS-VILAR, I., ALMÉCIJA, S., ROBLES, J.M., ARIAS-

878   MARTORELL, J. and MOYÀ-SOLÀ, S. 2012*b*. New dental remains of

879   *Hispanopithecus laietanus* (Primates: Hominidae) from Can Llobateres 1 and

880   the taxonomy of Late Miocene hominoids from the Vallès-Penedès Basin (NE

881   Iberian Peninsula). *Journal of Human Evolution*, **63**, 231–246.

882 — ALMÉCIJA, S., CASANOVAS-VILAR, I., MÉNDEZ, J.M., MOYÀ-SOLÀ, S.

883   2012*c*. A partial skeleton of *Hispanopithecus laietanus* from Can Feu and the

884   mosaic evolution of crown-hominoid positional behaviors. *PLoS ONE*, **7**,

885   e39617.

886 — FORTUNY, J., PÉREZ DE LOS RÍOS, M., ZANOLLI, C., ALMÉCIJA, S.,

887   CASANOVAS-VILAR, I., ROBLES, J.M. and MOYÀ-SOLÀ, S. 2013. New

888   dental remains of *Anoiapithecus* and the first appearance datum of hominoids

889   in the Iberian Peninsula. *Journal of Human Evolution,* **65**, 573–584.

890 — ALMÉCIJA, S., DEMIGUEL, D., FORTUNY, J., PÉREZ DE LOS RÍOS, M.,

891   PINA, M., ROBLES, J.M. and MOYÀ-SOLÀ, S. 2015. Miocene small-bodied

892   ape from Eurasia sheds light on hominoid evolution. *Science,* **350**, aab2625.

893 — CASANOVAS-VILAR, I., GARCÉS, M. and ROBLES, J.M. 2017. Ten years in

894   the dump: An updated review of the Miocene primate-bearing localities from

895   Abocador de Can Mata (NE Iberian Peninsula). *Journal of Human Evolution,*

896   **102**, 12–20.

897 — FORTUNY, J., ROBLES, J.M., BERNARDINI, F., PÉREZ DE LOS RÍOS, M.,

898   TUNIZ, C., MOYÀ-SOLÀ, S. and ZANOLLI, C. 2020. A new dryopithecine

899   mandibular fragment from the middle Miocene of Abocador de Can Mata and

900   the taxonomic status of 'Sivapithecus' *occidentalis* from Can Vila (Vallès-

901   Penedès Basin, NE Iberian Peninsula. *Journal of Human Evolution*, **145**,

902   102790.

903 ALMÉCIJA, S., ALBA, D. M., MOYÀ-SOLÀ, S., and KÖHLER, M. 2007. Orang-

904   like manual adaptations in the fossil hominoid *Hispanopithecus laietanus*: first

905   steps towards great ape suspensory behaviours. *Proceedings of the Royal*

906   *Society B*, **274**, 2375–2384.

907 — — — 2009. *Pierolapithecus* and the functional morphology of Miocene ape hand

908   phalanges: paleobiological and evolutionary implications. *Journal of Human*

909   *Evolution*, **57**, 284–297.

910 — TALLMAN, M., ALBA, D.M., PINA, M., MOYÀ-SOLÀ, S., and JUNGERS,

911   W.L. 2013. The femur of *Orrorin tugenensis* exhibits morphometric affinities

912   with both Miocene apes and later hominins. *Nature Communications*, **4**, 2888.

913 ANDREWS, P., 2020. Last common ancestor of apes and humans: Morphology and

914   environment. *Folia Primatologica*, **91**, 122–148.

915 — and MARTIN, L. 1991. Hominoid dietary evolution. *Philosophical Transactions of*

916   *the Royal Society B,* **334**, 199–209.

917 — HARRISON, T., DELSON, E., BERNOR, R. L. and MARTIN, L. 1996.

918   Distribution and biochronology of European and Southwest Asian Miocene

919   catarrhines. 168–207. *In* BERNOR, R.L., FAHLBUSCH, V. and

920   MITTMANN, H.-W (eds). *The Evolution of Western Eurasian Neogene*

921   *Mammal Faunas*. Columbia University Press, Columbia, 528 pp.

922 BAYLE, P., BONDIOLI, L., MACCHIARELLI, R., MAZURIER, A., PUYMERAIL,

923   L., VOLPATO, V. and ZANOLLI, C. 2011. Three-dimensional imaging and

924   quantitative characterization of human fossil remains. Examples from the

925   Nespos database. 29–46. *In* MACCHIARELLI, R. and WENIGER G.-C. (eds).

926   *Pleistocene Databases. Acquisition, Storing, Sharing.* Wissenschaftliche

927   Schriften des Neanderthal Museums, Mettmann **4**, 121 pp.

928 BEGUN, D.R. 1992. *Dryopithecus crusafonti* sp. nov., a new Miocene hominoid

929   species from Can Ponsic (Northeastern Spain). *American Journal of Physical*

930   *Anthropology,* **87**, 291–309.

931 — 2002. European hominoids. 339–368. *In* HARTWIG, W.C. (ed). *The Primate*

932   *Fossil Record*. Cambridge University Press, Cambridge, 503 pp.

933 — 2003. Planet of the apes. *Scientific American*, **289**, 74–83.

934 — 2007. Fossil record of Miocene hominoids. 921–977. *In* HENKE, W. and

935   TATTERSALL, I. (eds). *Handbook of Paleoanthropology*. Springer Verlag,

936   Berlin, 2069 pp.

937 — 2009. Dryopithecins, Darwin, de Bonis, and the European origin of the African

938   apes and human clade. *Geodiversitas,* **31**, 789–816.

939 — 2010. Miocene hominids and the origins of the African apes and humans. *Annual*

940   *Review of Anthropology*, **39**, 67–84.

941 — 2015. Fossil record of Miocene hominoids. 1261–1332. *In* HENKE, W. and

942   TATTERSALL, I. (eds). *Handbook of Paleoanthropology.* Springer Verlag,

943   Berlin, 2624 pp.

944 — MOYA-SOLA, S. and KOHLER, M. 1990. New Miocene hominoid specimens

945   from Can Llobateres (Vallès Penedès, Spain) and their geological and

946   paleoecological context. *Journal of Human Evolution,* **19**, 255–268.

947 — NARGOLWALLA, M. C. and KORDOS, L. 2012. European Miocene hominids

948   and the origin of the African ape and human clade. *Evolutionary Anthropology*,

949   **21**, 10–23.

950 BENAZZI, S., PANETTA, D., FORNAI, C., TOUSSAINT, M., GRUPPIONI, G. and

951   HUBLIN, J.J. 2014. Guidelines for the digital computation of 2D and 3D

952   enamel thickness in hominoid teeth. *American Journal of Physical*

953   *Anthropology,* **153**, 305–313.

954 BÖHME, M., SPASSOV, N., FUSS, J., TRÖSCHER, A., DEANE, A.S., PRIETO, J.,

955   KIRSCHER, U., LECHNER, T. and BEGUN, D.R., 2019. A new Miocene ape

956   and locomotion in the ancestor of great apes and humans. *Nature,* **575**, 489–

957   493.

958 CAMERON, D.W. 1997. A revised systematic scheme for the Eurasian Miocene fossil

959   Hominidae. *Journal of Human Evolution*, **33**, 449–477.

960 — 1998. Patterns of faciodental sexual dimorphism in *Hispanopithecus*. *Zeitschrift für*

961   *Morphologie und Anthropologie*, **82**, 47–58.

962 — 1999. The single species hypothesis and *Hispanopithecus* fossils from the Vallés

963   Penedés Basin, Spain. *Zeitschrift für Morphologie und Anthropologie*, **82**,

964   159–186.

965 CASANOVAS-VILAR, I., ALBA, D.M., GARCÉS, M., ROBLES, J.M. and MOYÀ-

966   SOLÀ, S. 2011. Updated chronology for the Miocene hominoid radiation in

967   Western Eurasia. *Proceedings of the National Academy of Sciences of the*

968   *United States of America,* **108**, 5554–5559.

969 — GARCÉS, M., VAN DAM, J.A., GARCÍA PAREDES, I., ROBLES, J.M. and

970 ALBA, D.M. 2016. An updated biostratigraphy for the late Aragonian and

971 Vallesian of the Vallès-Penedès Basin (Catalonia). *Geologica Acta,* **14**, 195–

972 217.

973 COLEMAN, M.N. and COLBERT, M.W. 2007. CT thresholding protocols for taking

974 measurements on three-dimensional models. *American Journal of Physical*

975 *Anthropology,* **133**, 723–725.

976 CRUSAFONT-PAIRO, M. and HÜRZELER, J., 1961. Les Pongidés fossiles

977 d'Espagne. *Comptes Rendus de l'Académie des Science*, Paris **252**, 582–584.

978 — — 1969. Catálogo comentado de los póngidos fósiles de España. *Acta Geologica*

979 *Hispánica*, **4**, 44–48.

980 — and GOLPE-POSSE, J.M. 1973. New pongids from the Miocene of Vallès Penedès

981 Basin (Catalonia, Spain). *Journal of Human Evolution*, **2**, 17–24.

982 DAVIES, T.W., DELEZENE, L. K., GUNZ, P., HUBLIN, J.-J. and SKINNER, M. M.

983 2019. Endostructural morphology in hominoid mandibular third premolars:

984 Discrete traits at the enamel-dentine junction. *Journal of Human Evolution*,

985 **136**, 102670.

986 DEMIGUEL, D., ALBA, D.M. and MOYÀ-SOLÀ, S. 2014. Dietary specialization

987 during the evolution of Western Eurasian hominoids and the extinction of

988 European great apes. *PLoS One,* **9**, e97442.

989 DETROIT, F., MIJARES, A.S., CORNY, J., DAVER, G., ZANOLLI, C., DIZON, E.,

990 ROBLES, E., GRÜN, R. and PIPER, P.J. 2019. A new species of *Homo* from

991 the Late Pleistocene of the Philippines. *Nature,* **568**, 181–186.

992 FAJARDO, R.J., RYAN, T.M. and KAPPELMAN J. 2002. Assessing the accuracy of

993 high resolution X-ray computed tomography of primate trabecular bone by

994   comparisons with histological sections. *American Journal of Physical*

995   *Anthropology,* **118**, 1–10.

996   FLEAGLE, J.G. 2013. *Primate Adaptation and Evolution*, 3rd ed. Academic Press,

997   London, 464 pp.

998   FORTUNY, J., ZANOLLI, C., BERNARDINI, F., TUNIZ, C. and ALBA, D.M. 2020.

999   Data from: Dryopithecine palaeobiodiversity in the Iberian Miocene revisited

1000   on the basis of molar endostructural morphology. *Dryad Digital Repository*.

1001   https://datadryad.org/stash/share/EiJrlF8TAY9FmzkrKqbzIcaiXBO8BD-

1002   b1BSPjduY8Eg

1003   GOLPE-POSSE, J.M. 1993. Los Hispanopitecos (Primates, Pongidae) de los

1004   yacimientos del Vallès-Penedès (Cataluña, España). II: Descripción del

1005   material existente en el Instituto de Paleontología de Sabadell. *Paleontologia i*

1006   *Evolució*, **26–27**, 151–224.

1007   GRINE, F.E. 2002. Scaling of tooth enamel thickness, and molar crown size reduction

1008   in modern humans. *South African Journal of Science*, **98**, 503–509.

1009   ─ 2005. Enamel thickness of deciduous and permanent molars in modern *Homo*

1010   *sapiens*. *American Journal of Physical Anthropology*, **126**, 14–31.

1011   GRINE, F.E. and DAEGLING, D.J. 2017. Functional morphology, biomechanics and

1012   the retrodiction of early hominin diets. *Comptes Rendus Palevol*, **16**, 613–631.

1013   ─ and MARTIN, L.B. 1988. Enamel thickness and development in *Australopithecus*

1014   and *Paranthropus*. 3–42. *In* GRINE, F.E (ed). *Evolutionary History of the*

1015   *"Robust" Australopithecines*. Aldine de Gruyter, Berlin, 550 pp.

1016   HAMMER, Ø., HARPER, D.A.T. and RYAN, P.D. 2001. PAST: Paleontological

1017   statistics software package for education and data analysis. *Palaeontologia*

1018   *Electronica*, **4**, 4.

1019   HARRISON, T. 1991. Some observations on the Miocene hominoids from Spain.

1020   *Journal of Human Evolution*, **19**, 515–520.

1021   ― and GU, Y. 1999. Taxonomy and phylogenetic relationships of early Miocene

1022   catarrhines from Sihong, China. *Journal of Human Evolution,* **37**, 225–277.

1023   KELLEY, J. DEAN, M.C. and REID, D.J. 2001. Molar growth in the late Miocene

1024   hominoid, *Dryopithecus laietanus*. 123–134. *In* BROOK, A. (ed). *Dental*

1025   *Morphology 2001: 12th International Symposium on Dental Morphology*.

1026   Sheffield Academic Press, Sheffield, 350 pp.

1027   KONO, R. 2004. Molar enamel thickness and distribution patterns in extant great apes

1028   and humans: New insights based on a 3-dimensional whole crown perspective.

1029   *Anthropological Science*, **112**, 121–146.

1030   ― and SUWA, G. 2008. Enamel distribution patterns of extant human and hominoid

1031   molars: Occlusal versus lateral enamel thickness. *Bulletin of the National*

1032   *Museum of Nature and Science, Series D*, **34**, 1–9.

1033   KUPCZIK, K. and HUBLIN, J.J. 2010. Mandibular molar root morphology in

1034   Neanderthals and Late Pleistocene and recent *Homo sapiens*. *Journal of*

1035   *Human Evolution*, **59**, 525–541.

1036   ― DELEZENE, L.K. and SKINNER, M.M. 2019. Mandibular molar root and pulp

1037   cavity morphology in Homo naledi and other Plio-Pleistocene hominins.

1038   *Journal of Human Evolution*, **130**, 83–95.

1039   MACCHIARELLI, R., BONDIOLI, L. and MAZURIER, A. 2008. Virtual dentitions:

1040   touching the hidden evidence. 426–448. *In* IRISH, J.D., NELSON, G.C. (eds),

1041   *Technique and Application in Dental Anthropology*. Cambridge University

1042   Press, Cambridge, 470 pp.

1043   — MAZURIER, M., ILLERHAUS, B. and ZANOLLI, C. 2009. *Ouranopithecus*

1044   *macedoniensis*: virtual reconstruction and 3D analysis of a juvenile mandibular

1045   dentition (RPl-82 and RPl-83). *Geodiversitas,* **31**, 851–863.

1046   — BAYLE, P., BONDIOLI, L., MAZURIER, A., ZANOLLI, C. 2013. From outer to

1047   inner structural morphology in dental anthropology: integration of the third

1048   dimension in the visualization and quantitative analysis of fossil remains. 250–

1049   277. *In* SCOTT, G.R. and IRISH, J.D. (eds), *Anthropological Perspectives on*

1050   *Tooth Morphology. Genetics, Evolution, Variation.* Cambridge University

1051   Press, Cambridge, 582 pp.

1052   MACHO, G.A. 1994. Variation in enamel thickness and cusp area within human

1053   maxillary molars and its bearing on scaling techniques used for studies of

1054   enamel thickness between species. *Archives of Oral Biology*, **39**, 783–792.

1055   MARIGÓ, J., SUSANNA, I., MINWER-BARAKAT, R., MADURELL-

1056   MALAPEIRA, J., MOYÀ-SOLÀ, S., CASANOVAS-VILAR, I., ROBLES,

1057   J.M. and ALBA, D.M. 2014. The primate fossil record in the Iberian

1058   Peninsula. *Journal of Iberian Geology*, **40**, 179–211.

1059   MARTIN, L.B. 1985. Significance of enamel thickness in hominoid evolution. *Nature*

1060   **314**, 260–263.

1061   MARTIN-FRANCÉS, L., MARTINÓN-TORRES, M., MARTÍNEZ DE PINILLOS,

1062   M., GARCÍA-CAMPOS, C., MODESTO-MATA, M., ZANOLLI, C.,

1063   RODRÍGUEZ, L. and BERMUDEZ DE CASTRO, J.M. 2018. Tooth crown

1064   tissue proportions and enamel thickness in Early Pleistocene Homo antecessor

1065   molars (Atapuerca, Spain). PLoS ONE*,* **13,** e0203334.

1066 MOORE, N.C., SKINNER, M.M. and HUBLIN, J.J. 2013. Premolar root morphology
1067   and metric variation in *Pan troglodytes verus*. *American Journal of Physical*
1068   *Anthropology*, **150**, 632–646.

1069 — THACKERAY, J.F., HUBLIN, J.J. and SKINNER, M.M. 2016. Premolar root and
1070   canal variation in South African Plio-Pleistocene specimens attributed to
1071   *Australopithecus africanus* and *Paranthropus robustus*. *Journal of Human*
1072   *Evolution*, **93**, 46–62.

1073 MOYÀ-SOLÀ, S. and KÖHLER, M. 1993. Recent discoveries of *Dryopithecus* shed
1074   new light on evolution of great apes. *Nature,* **365**, 543–545.

1075 — — 1995. New partial cranium of *Dryopithecus* Lartet, 1863 (Hominoidea,
1076   Primates) from the upper Miocene of Can Llobateres, Barcelona, Spain.
1077   *Journal of Human Evolution*, **29**, 101–139.

1078 — — ALBA, D.M., CASANOVAS-VILAR, I. and GALINDO, J. 2004.
1079   *Pierolapithecus catalaunicus*, a new Middle Miocene great ape from Spain.
1080   *Science,* **306**, 1339–1344.

1081 — — ALBA, D.M., CASANOVAS-VILAR, I. and GALINDO, J. 2005. Response to
1082   comment on "*Pierolapithecus catalaunicus*, a new Middle Miocene great ape
1083   from Spain". *Science,* **308**, 203d.

1084 — ALBA, D.M., ALMÉCIJA, S., CASANOVAS-VILAR, I., KÖHLER, M., DE
1085   ESTEBAN-TRIVIGNO, S., ROBLES, J.M., GALINDO, J. and FORTUNY, J.
1086   2009*a*. A unique Middle Miocene European hominoid and the origins of the
1087   great ape and human clade. *Proceedings of the National Academy of Sciences*
1088   *of the United States of America,* **106**, 9601–9606.

1089 — KÖHLER, M., ALBA, D.M., CASANOVAS-VILAR, I., GALINDO, J., ROBLES,
1090   J.M., CABRERA, L., GARCÉS, M., ALMÉCIJA, S. and BEAMUD, E.

1091   2009*b*. First partial face and upper dentition of the Middle Miocene hominoid

1092   *Dryopithecus fontani* from Abocador de Can Mata (Vallès-Penedès Basin,

1093   Catalonia, NE Spain): taxonomic and phylogenetic implications. *American*

1094   *Journal of Physical Anthropology*, **139**, 126–145.

1095 OLEJNICZAK, A.J. 2006. Micro-computed tomography of primate molars.

1096   Unpublished PhD thesis, Stony Brook University, New York, 242 pp.

1097 — MARTIN, L.B. and ULHAAS, L. 2004. Quantification of dentine shape in

1098   anthropoid primates. *Annals of Anatomy*, **186**, 479–486.

1099 — TAFFOREAU, P., FEENEY, R.N.M. and MARTIN, L.B. 2008*a*. Three-

1100   dimensional primate molar enamel thickness. *Journal of Human Evolution*, **54**,

1101   187–195.

1102 — — — — 2008*b*. Three-dimensional molar enamel distribution and thickness in

1103   *Australopithecus* and *Paranthropus*. *Biology Letters*, **4**, 406–410.

1104 — SMITH, T.M., WANG, W., POTTS, R., CIOCHON, R., KULLMER, O.,

1105   SCHRENK, F. AND HUBLIN, J.-J. 2008*c*. Molar enamel thickness and

1106   dentine horn height in *Gigantopithecus blacki*. *American Journal of Physical*

1107   *Anthropology*, **135**, 85–91.

1108 — — T.M., FEENEY, R.N., MACCHIARELLI, R., MAZURIER, A., BONDIOLI,

1109   L., ROSAS, A., FORTEA, J., DE LA RASILLA, M., GARCIA-

1110   TABERNERO, A., RADOVCIC, J., SKINNER, M.M., TOUSSAINT M., and

1111   HUBLIN, J.-J. 2008*d*. Dental tissue proportions and enamel thickness in

1112   Neandertal and modern human molars. *Journal of Human Evolution,* **55**, 12–

1113   23.

1114 PAN, L., DUMONCEL, J., MAZURIER, A. and ZANOLLI, C. 2019. Structural

1115   analysis of premolar roots in Middle Pleistocene hominins from China. *Journal*

1116   *of Human Evolution,* **136**, 102669

1117 PÉREZ DE LOS RÍOS, M., MOYÀ-SOLÀ, S. and ALBA, D.M. 2012. The nasal and

1118   paranasal architecture of the Middle Miocene ape *Pierolapithecus catalaunicus*

1119   (Primates: Hominidae): Phylogenetic implications. *Journal of Human*

1120   *Evolution,* **63**, 497–506.

1121 — ALBA, D.M. and MOYÀ-SOLÀ, S., 2013. Taxonomic attribution of the La Grive

1122   hominoid teeth. *American Journal of Physical Anthropology*, **151**, 558–565.

1123 PICKFORD, M. 2012. Hominoids from Neuhausen and other Bohnerz localities,

1124   Swabian Alb, Germany: evidence for a high diversity of apes in the Late

1125   Miocene of Germany. *Estudios Geológicos*, **68**, 113–147.

1126 PINA, M., ALBA, D.M., ALMÉCIJA, S., FORTUNY, J., and MOYÀ-SOLA, S.

1127   2012. Brief Communication: Paleobiological inferences on the locomotor

1128   repertoire of extinct hominoids based on femoral neck cortical thickness: the

1129   fossil great ape *Hispanopithecus laietanus* as a test-case study. *American*

1130   *Journal of Physical Anthropology*, **149**, 142–148.

1131 — — MOYÀ-SOLÀ, S., and ALMÉCIJA, S. 2019. Femoral neck cortical bone

1132   distribution of dryopithecin apes and the evolution of hominid locomotion.

1133   *Journal of Human Evolution*, **136**, 102651.

1134 RIBOT, F., GIBERT, J. and HARRISON, T. 1996. A reinterpretation of the taxonomy

1135   of *Dryopithecus* from Vallès-Penedès, Catalonia (Spain). *Journal of Human*

1136   *Evolution,* **31**, 129–141.

1137 SCHNEIDER, C.A., RASBAND, W.S. and ELICEIRI, K.W. 2012. NIH Image to

1138   ImageJ: 25 years of image analysis. *Nature Methods,* **9**, 671–675.

1139   SCHWARTZ, G.T. 2000. Taxonomic and functional aspects of the patterning of

1140   enamel thickness distribution in extant large-bodied hominoids. *American*

1141   *Journal of Physical Anthropology*, **111**, 221–244.

1142   SCOTT, G.R and IRISH J.D. 2017. *Human Tooth Crown and Root Morphology. The*

1143   *Arizona State University Dental Anthropology System*. Cambridge University

1144   Press, Cambridge, 342 pp.

1145   SIMONS, E. L. and PILBEAM, D. R. 1965. Preliminary revision of the

1146   Dryopithecinae (Pongidae, Anthropoidea). *Folia Primatologica*, **3**, 81–152.

1147   SKINNER, M. M. 2008. Enamel-dentine junction morphology of extant hominoid and

1148   fossil hominin lower molars. Unpublished Ph.D thesis, The George

1149   Washington University, Washington D.C., 191 pp.

1150   — WOOD, B.A., BOESCH, C., OLEJNICZAK, A., ROSAS, A., SMITH, T.M., and

1151   HUBLIN, J.-J. 2008*a*. Dental trait expression at the enamel-dentine junction of

1152   lower molars in extant and fossil hominoids. *Journal of Human Evolution,* **54**,

1153   173–186.

1154   — GUNZ, P., WOOD, B. A. and HUBLIN, J.-J. 2008*b*. Enamel-dentine junction

1155   (EDJ) morphology distinguishes the lower molars of *Australopithecus*

1156   *africanus* and *Paranthropus robustus*. *Journal of Human Evolution,* **55**, 979–

1157   988.

1158   — WOOD, B.A. and HUBLIN, J.-J. 2009*a*. Protostylid expression at the enamel-

1159   dentine junction and enamel surface of mandibular molars of *Paranthropus*

1160   *robustus* and *Australopithecus africanus*. *Journal of Human Evolution,* **56**, 76–

1161   85.

1162   — GUNZ, P., WOOD, B. A., BOESCH, C. and HUBLIN, J.-J. 2009*b*. Discrimination

1163   of extant *Pan* species and subspecies using the enamel-dentine junction

morphology of lower molars. *American Journal of Physical Anthropology,* **140**, 234–243.

— DE VRIES, D., GUNZ, P., KUPCZIK, K., KLASSEN, R.P., HUBLIN, J.J. and ROKSANDIC, M. 2016. A dental perspective on the taxonomic affinity of the Balanica mandible (BH-1). *Journal of Human Evolution,* **93**, 63–81.

SMITH, H.B. 1984. Patterns of molar wear in hunter-gatherers and agriculturalists. *American Journal of Physical Anthropology,* **63**, 39–56.

SMITH, T.M., OLEJNICZAK, A.J., MARTIN, L.B. and REID, D.J. 2005. Variation in hominoid molar enamel thickness. *Journal of Human Evolution,* **48**, 575–592.

— — REID, D.J., FERRELL, R.J. and HUBLIN J.-J. 2006. Modern human molar enamel thickness and enamel-dentine junction shape. *Archives of Oral Biology*, **51**, 974–995.

— — REH, S., REID, D.J. and HUBLIN, J.-J. 2008. Enamel thickness trends in the dental arcade of humans and chimpanzees. *American Journal of Physical Anthropology,* **136**, 237–241.

— — ZERMENO, J.P., TAFFOREAU, P., SKINNER, M.M., HOFFMANN, A., RADOVČIĆ, J., TOUSSAINT, M., KRUSZYNSKI, R., MENTER, C., MOGGI-CECCHI, J., GLASMACHER, U.A., KULLMER, O., SCHRENK, F., STRINGER, C. and HUBLIN, J.J. 2012a. Variation in enamel thickness within the genus *Homo Journal of Human Evolution,* **62***,* 395–411

— KUPCZIK, K., MACHANDA, Z., SKINNER, M.M. and ZERMENO, J.P. 2012b. Enamel thickness in Bornean and Sumatran orangutan dentitions. *American Journal of Physical Anthropology,* **147**, 417–426.

1188 — TAFFOREAU, P., POUECH, J. and BEGUN, D.R. 2019. Enamel thickness and

1189   dental development in *Rudapithecus hungaricus*. *Journal of Human Evolution*,

1190   **136**, 102649.

1191 SPOOR, F., ZONNEVELD, F. and MACHO, G.A. 1993. Linear measurements of

1192   cortical bone and dental enamel by computed tomography: applications and

1193   problems. *American Journal of Physical Anthropology,* **91**, 469–484.

1194 SUWA, G. and KONO, R. T. 2005. A micro-CT based study of linear enamel

1195   thickness in the mesial cusp section of human molars: Reevaluation of

1196   methodology and assessment of within-tooth, serial, and individual variation.

1197   *Anthropological Sciencies*, **113**, 273–289.

1198 SUWA, G., KONO, R.T., SIMPSON, S.W., ASFAW, B., LOVEJOY, C.O. and

1199   WHITE, T. 2009. Paleobiological implications of the *Ardipithecus ramidus*

1200   dentition. *Science,* **326**, 94–99.

1201 SWINDLER, D.R. 2002. *Primate Dentition. An Introduction to the Teeth of Non-*

1202   *Human Primates*. Cambridge University Press, Cambridge, 296 pp.

1203 THIERY, G., LAZZARI, V., RAMDARSHAN, A. and GUY, F. 2017. Beyond the

1204   map: Enamel distribution characterized from 3D dental topography. *Frontiers*

1205   *in Physiology*, **8**, 524.

1206 TURNER, C.G. NICHOL, C.R. and SCOTT, G.R. 1991. Scoring procedures for key

1207   morphological traits of the permanent dentition: The Arizona State University

1208   Dental Anthropology System. 13–31. *In* KELLEY, L., KELLEY, M. and

1209   LARSEN, C.S. (eds), *Advances in Dental Anthropology*. Wiley-Liss, New

1210   York, 389 pp.

1211 TUNIZ, C., BERNARDINI, F., CICUTTIN, A., CRESPO, M.-L., DREOSSI, D.,

1212   GIANONCELLI, A., MANCINI, L., MENDOZA CUEVAS, A., SODINI, N.,

1213   TROMBA, G., ZANINI, F. and ZANOLLI, C. 2013.The ICTP-Elettra X-ray

1214   laboratory for cultural heritage and archaeology. A facility for training and

1215   education in the developing world. *Nuclear Instruments and Methods in*

1216   *Physics Research Section A*, **711**, 106–110.

1217 VAN DER MADE, J. and RIBOT, F. 1999. Additional hominoid material from the

1218   Miocene of Spain and remarks on hominoid dispersals into Europe.

1219   *Contributions to Tertiary and Quaternary Geology,* **36**, 25–39.

1220 VILLALTA COMELLA, J.F. DE and CRUSAFONT PAIRO, M. 1941. Hallazgo del

1221   "*Dryopithecus fontani*", Lartet, en el Vindoboniense de la cuenca Vallés-

1222   Penedés. *Boletín Instituto Geológico y Minero de España*, **55**, 131–142.

1223 — — 1944. Dos nuevos antropomorfos del Mioceno español y su situación dentro de

1224   la moderna sistemática de los símidos. *Notas y Comunicaciones del Instituto*

1225   *Geológico y Minero de España*, **13**, 1–51.

1226 VOGEL, E.R., VAN WOERDEN, J.T., LUCAS, P.W., UTAMI ATMOKO, S.S.,

1227   VAN SCHAIK, C.P. and DOMINY, N.J. 2008. Functional ecology and

1228   evolution of hominoid molar enamel thickness: *Pan troglodytes schweinfurthii*

1229   and *Pongo pygmaeus wurmbii*. *Journal of Human Evolution*, **55**, 60–74.

1230 ZANOLLI, C., BONDIOLI, L., MANCINI, L., MAZURIER, A., WIDIANTO, H. and

1231   MACCHIARELLI, R. 2012. Two human fossil deciduous molars from the

1232   Sangiran Dome (Java, Indonesia): Outer and inner morphology. *American*

1233   *Journal of Physical Anthropology,* **147**, 472–481.

1234 — and MAZURIER, A. 2013. Endostructural characterization of the *H.*

1235   *heidelbergensis* dental remains from the early Middle Pleistocene site of

1236   Tighenif, Algeria. *Comptes Rendus Palevol*, **12**, 293–304.

1237   — BONDIOLI, L., COPPA, A., DEAN, C.M., BAYLE, P., CANDILIO, F.,

1238   CAPUANI, S., DREOSSI, D., FIORE, I., FRAYER, D.W., LIBSEKAL, Y.,

1239   MANCINI, L., ROOK, L., MEDIN TEKLE, T., TUNIZ, C. and

1240   MACCHIARELLI, R. 2014. The late Early Pleistocene human dental remains

1241   from Uadi Aalad and Mulhuli-Amo (Buia), Eritrean Danakil:

1242   macromorphology and microstructure. *Journal of Human Evolution*, **74**, 96–

1243   113.

1244   — DEAN, C.M., ROOK, L., BONDIOLI, L., MAZURIER, A. and

1245   MACCHIARELLI, R. 2016. Enamel thickness and enamel growth in

1246   *Oreopithecus*: Combining microtomographic and histological evidence.

1247   *Comptes Rendus Palevol,* **15**, 209–226.

1248   — PAN, L., DUMONCEL, J., KULLMER, O., KUNDRAT, M., LIU, W.,

1249   MACCHIARELLI, R., MANCINI, L., SCHRENK, F. and TUNIZ, C., 2018.

1250   Inner tooth morphology of *Homo erectus* from Zhoukoudian. New evidence

1251   from an old collection housed at Uppsala. *Journal of Human Evolution*, **116**,

1252   1–13.

1253   — KULLMER, O., KELLEY, J., BACON, A.-M., DEMETER, F., DUMONCEL, J.,

1254   FIORENZA, L., GRINE, F.E., HUBLIN, J.-J., TUAN NGUYEN, A., HUONG

1255   NGUYEN, T.M., PAN, L., SCHILLINGER, B., SCHRENK, F., SKINNER,

1256   M., JI, X. and MACCHIARELLI, R. 2019. Evidence for increased hominid

1257   diversity in the Early to Middle Pleistocene of Indonesia. *Nature Ecology and*

1258   *Evolution*, **3**, 755–764.

1259

1260   **FIGURE CAPTIONS**

1261   **Fig. 1.** Boxplots comparing relative enamel thickness among dryopithecine species

1262   recorded in NE Iberian Peninsula: (A) 2D RET; (B) 3D RET. Only taxa represented

1263   by at least three specimens are depicted. Boxes represent the interquartile range (IQR;

1264   25th and 75th percentiles), centerline is median, whiskers denote the maximum and

1265   minimum values within 1.5 times the IQR, dots are outliers, and stars represent

1266   extreme outliers. Abbreviations: PC, *Pierolapithecus catalaunicus*; DF, *Dryopithecus*

1267   *fontani*; AB, *Anoiapithecus brevirostris*; HC, *Hispanopithecus crusafonti*; HL,

1268   *Hispanopithecus laietanus*; SO, "*Sivapithecus*" *occidentalis* species inquirenda.

1269

1270   **Fig. 2.** Upper molar enamel distribution maps of Iberian dryopithecines. (A–C)

1271   *Pierolapithecus catalaunicus* (IPS21350, holotype): L M^1 (A), L M^2 (B), and L M^3

1272   (C); (D) *Dryopithecus fontani* (MGSB48486): R M^2; (E–G) *D. fontani* (IPS35026): L

1273 M^1 (E), L M^2 (F) and L M^3 (G); (H–L) *Anoiapithecus brevirostris* (IPS43000,

1274   holotype): R M^1 (H), R M^2 (I), R M^3 (J), L M^1 (K) and L M^2 (L); (M–P) *A.*

1275   *brevirostris* (IPS35027): L M^1 (M), L M^2 (N), R M^1 (O) and R M^2 (P); (Q–U)

1276   *Hispanopithecus crusafonti* (paratypes): L M^1 IPS1818 (Q), R M^1 IPS1815 (R), L M^2

1277   IPS1820 (S), R M^3 IPS1812 (T) and R M^3 IPS1814 (U); (V–Y) *Hispanopithecus*

1278   *laietanus*: R M^2 IPS1844 (V), L M^2 IPS58339 (W), L M^3 IPS58340 (X) and L M^3

1279   IPS1772 (Y). Each tooth has its own color scale of enamel thickness, ranging from 0

1280   to maximum thickness (indicated in mm above the scale). Scale bar represents 5 mm.

1281

1282   **Fig. 3.** Lower molar enamel distribution maps of Iberian dryopithecines. (A)

1283   "*Sivapithecus*" *occidentalis* species inquirenda (IPS41734): R M_2; (B–C) "*S.*"

1284   *occidentalis* (holotype): L M_2 IPS1826+1827 (B) and L M_3 IPS1826+1827 (C); (D–F)

1285   *Anoiapithecus brevirostris* (IPS43000, holotype): L M_1 (D), L M_2 (E), R M_1 (F); (G)

1286   *Hispanopithecus crusafonti* (IPS1816, paratype): R M_2; (H–J) *H. crusafonti*

1287   (MGSB25314): L M_1 (H), L M_2 (I) and L M_3 (J); (L–M) *Hispanopithecus laietanus*

1288   (IPS1804, holotype): L M_2 (L) and L M_3 (M); (K, N–S) *H. laietanus*: R M_2 IPS1780

1289   (K), R M_1 IPS1797 (N), R M_2 IPS1797 (O), R M_1 IPS1802 (P), R M_2 IPS1802 (Q), R

1290 M_3 IPS1802 (R) and L M_3 IPS1822 (S). Each tooth has its own color scale of enamel

1291   thickness, ranging from 0 to maximum thickness (indicated in mm above the scale).

1292   Scale bar represents 5 mm.

1293

1294   **Fig. 4.** Upper molar enamel-dentine junction (EDJ) Iberian dryopithecines. (A–C)

1295   *Pierolapithecus catalaunicus* (IPS21350, holotype): L M^1 (A), L M^2 (B), and L M^3

1296   (C); (D) *Dryopithecus fontani* (MGSB48486): R M^2; (E–G) *D. fontani* (IPS35026): L

1297 M^1 (E), L M^2 (F) and L M^3 (G); (H–L) *Anoiapithecus brevirostris* (IPS43000,

1298   holotype): R M^1 (H), R M^2 (I), R M^3 (J), L M^1 (K) and L M^2 (L); (M–P) *A.*

1299   *brevirostris* (IPS35027): L M^1 (M), L M^2 (N), R M^1 (O) and R M^2 (P); (Q–U)

1300   *Hispanopithecus crusafonti* (paratypes): L M^1 IPS1818 (Q), R M^1 IPS1815 (R), L M^2

1301   IPS1820 (S), R M^3 IPS1812 (T) and R M^3 IPS1814 (U); (V–Y) *Hispanopithecus*

1302   *laietanus*: R M^2 IPS1844 (V), L M^2 IPS58339 (W), L M^3 IPS58340 (X) and L M^3

1303   IPS1772 (Y). Scale bar represents 5 mm.

1304

1305   **Fig. 5.** Lower molar enamel-dentine junction (EDJ) of Iberian drypithecines. (A)

1306   "*Sivapithecus*" *occidentalis* species inquirenda (IPS41734): R M_2; (B–C) "*S.*"

1307   *occidentalis* (holotype): L M_2 IPS1826+1827 (B) and L M_3 IPS1826+1827 (C); (D–F)

1308   *Anoiapithecus brevirostris* (IPS43000, holotype): L M_1 (D), L M_2 (E), RM_1 (F); (G)

1309   *Hispanopithecus crusafonti* (IPS1816, paratype): R M_2; (H–J) *H. crusafonti*

1310   (MGSB25314): L M_1 (H), L M_2 (I) and L M_3 (J); (L–M) *Hispanopithecus laietanus*

1311   (IPS1804, holotype): L M$_2$ (L) and L M$_3$ (M); (K, N–S) *H. laietanus*: R M$_2$ IPS1780

1312   (K), R M$_1$ IPS1797 (N), R M$_2$ IPS1797 (O), R M$_1$ IPS1802 (P), R M$_2$ IPS1802 (Q), R

1313   M$_3$ IPS1802 (R) and L M$_3$ IPS1822 (S). Scale bar represents 5 mm.

1314

1315   **Table 1.** Studied samples of Miocene hominoids from Catalonia.

1316

1317   **Table 2.** Descriptive statistics for relative enamel thickness.

1318

1319   **Table 3.** Qualitative dental features of the EDJ of the upper molars.

1320

1321   **Table 4.** Qualitative dental features of the EDJ of the lower molars.
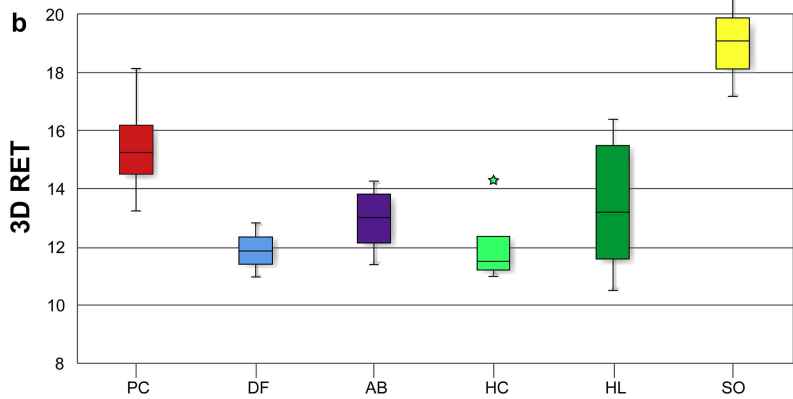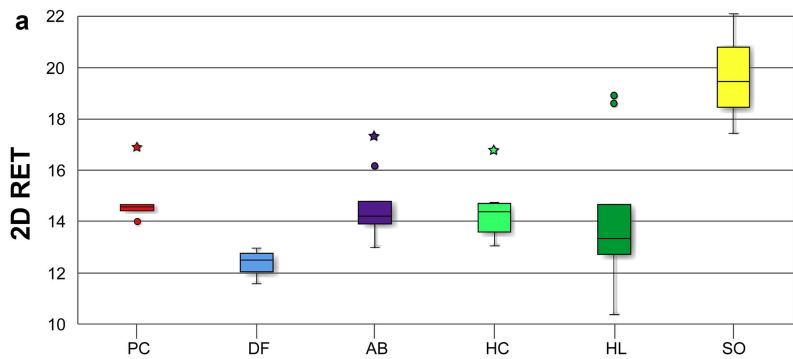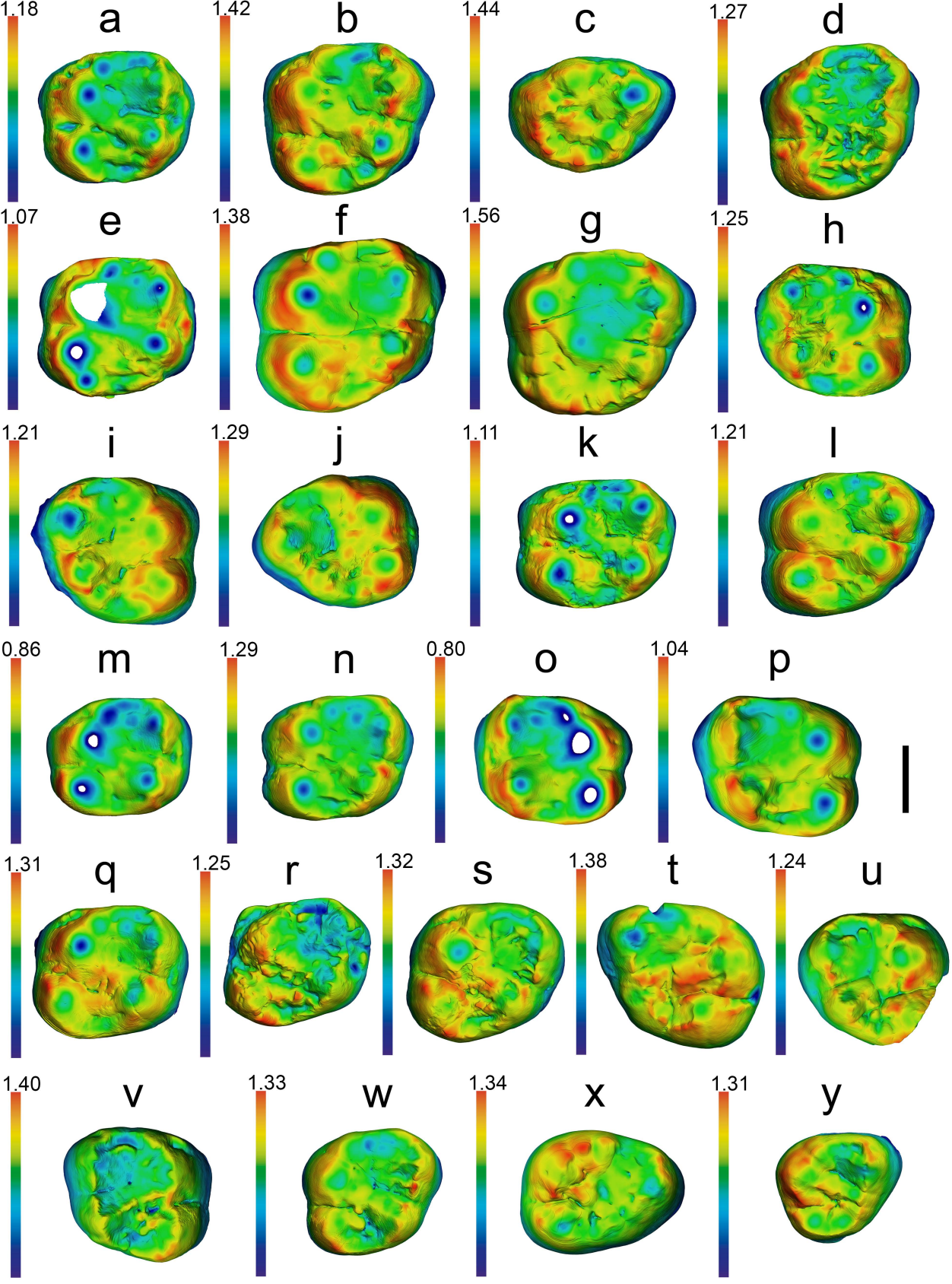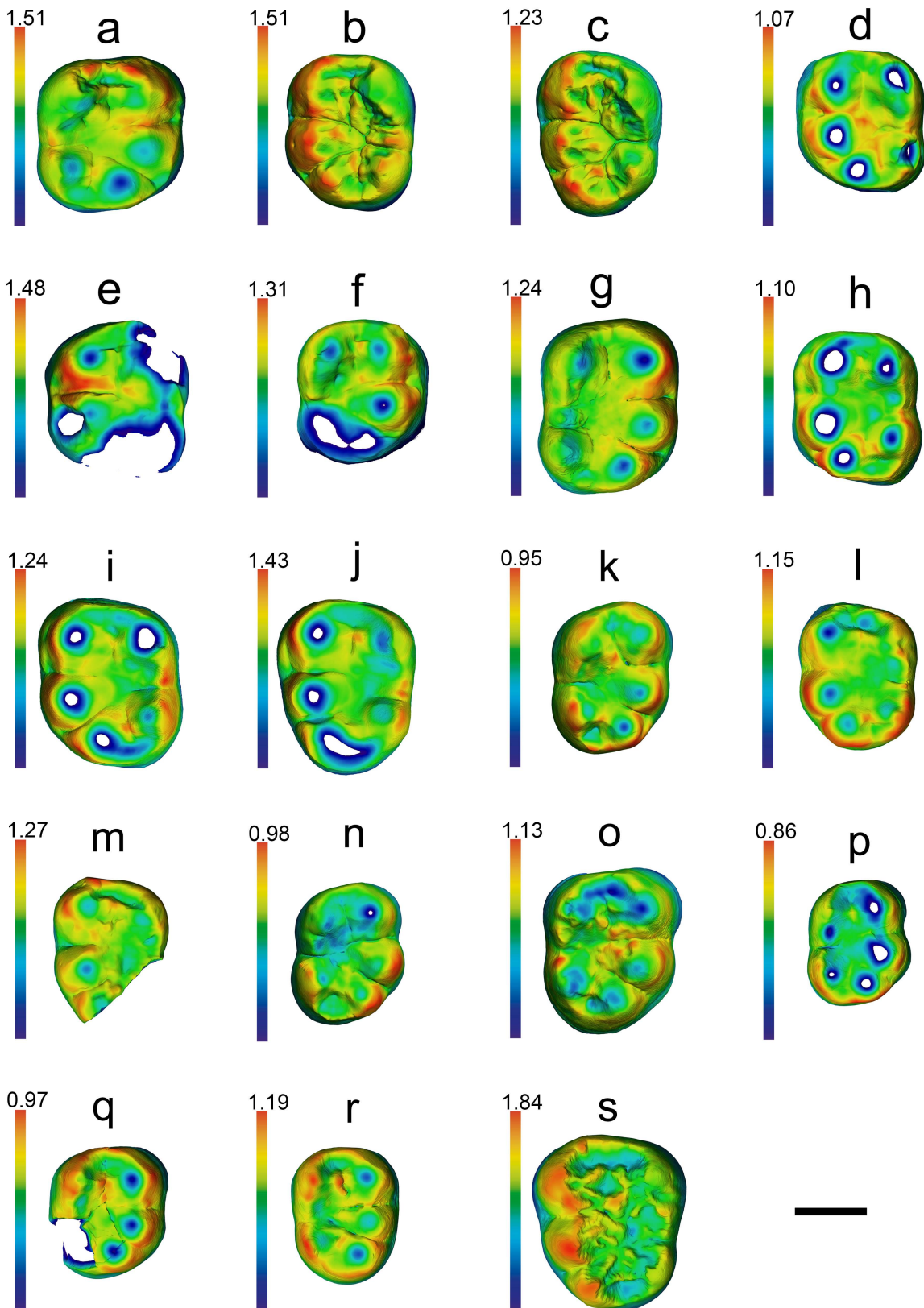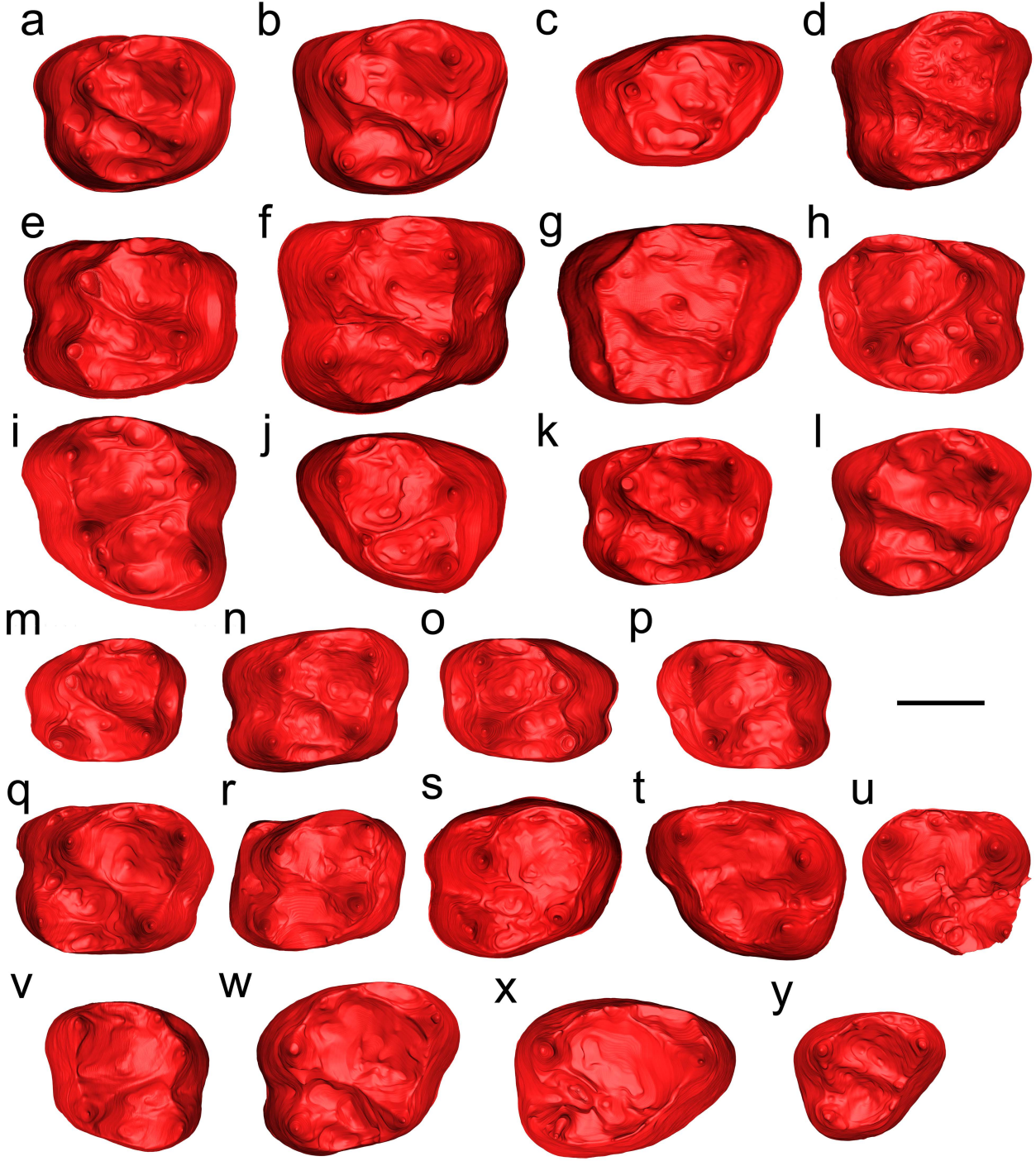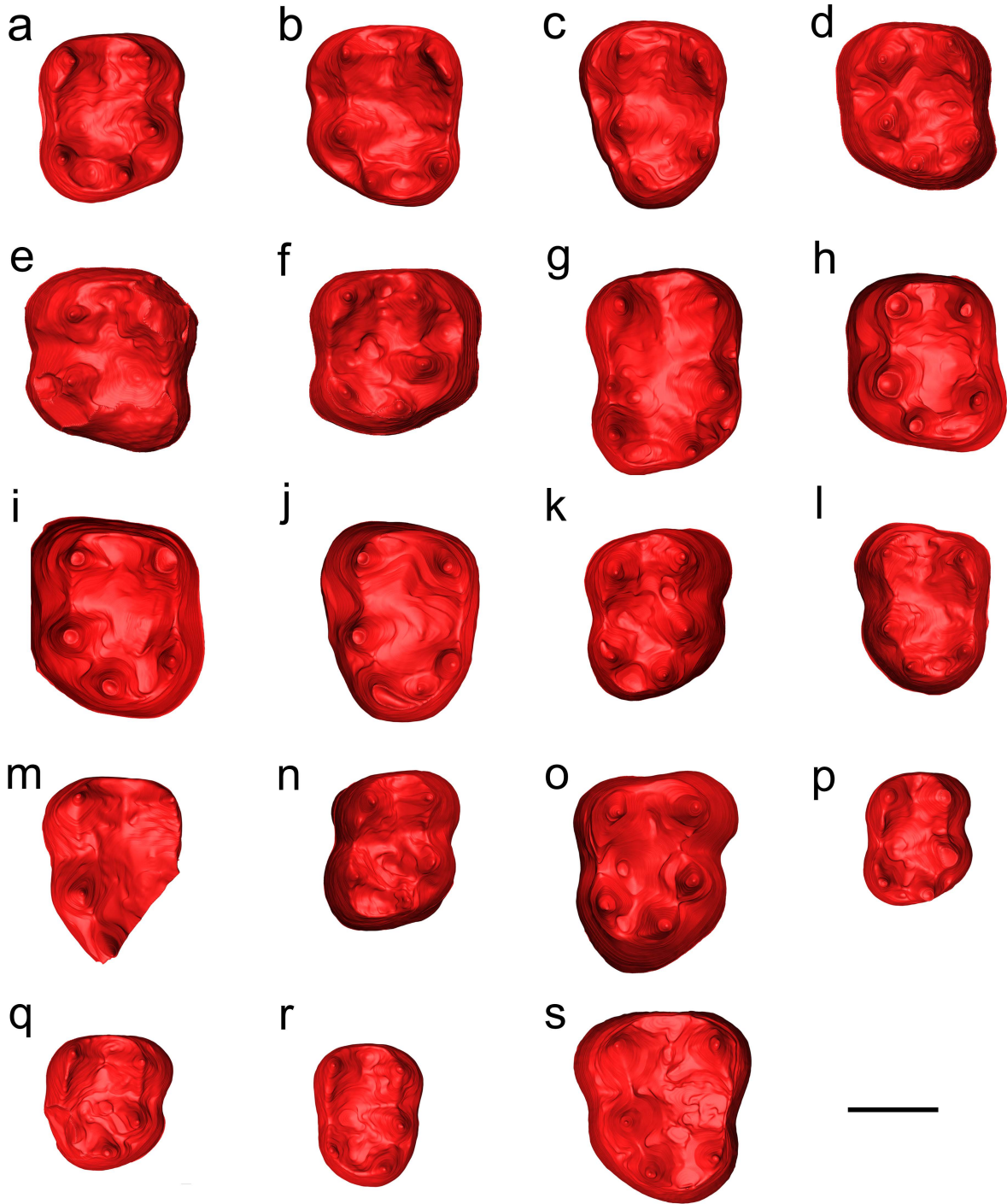
Table 1

Studied samples of Miocene hominoids from Catalonia.

Catalog No.	Tooth	Wear[a]	Locality	Age	Taxon	Remarks
IPS1772	L M^3	1–2	CLL1	9.7 Ma	*Hispanopithecus laietanus*	—
IPS1780	R M_2	1–2	CLL1	9.7 Ma	*Hispanopithecus laietanus*	—
IPS1797	R M_1	2–3	CLL1	9.7 Ma	*Hispanopithecus laietanus*	—
IPS1797	R M_2	1–2	CLL1	9.7 Ma	*Hispanopithecus laietanus*	—
IPS1802	R M_1	3	CLL1	9.7 Ma	*Hispanopithecus laietanus*	Invalid holotype of "*Rahonapithecus sabadellensis*" (nomen nudum)
IPS1802	R M_2	1–2	CLL1	9.7 Ma	*Hispanopithecus laietanus*	Invalid holotype of "*Rahonapithecus sabadellensis*" (nomen nudum)
IPS1802	R M_3	1–2	CLL1	9.7 Ma	*Hispanopithecus laietanus*	Invalid holotype of "*Rahonapithecus sabadellensis*" (nomen nudum)
IPS1804	L M_2	2	LT	9.5 Ma	*Hispanopithecus laietanus*	Holotype
IPS1804	L M_3	1–2	LT	9.5 Ma	*Hispanopithecus laietanus*	Holotype
IPS1812	R M^3	1	CP1	10.4–10.0 Ma	*Hispanopithecus crusafonti*	Paratype
IPS1814	R M^3	1–2	CP1	10.4–10.0 Ma	*Hispanopithecus crusafonti*	Paratype
IPS1815	L M^1	1–2	CP1	10.4–10.0 Ma	*Hispanopithecus crusafonti*	Paratype
IPS1816	R M_2	2	CP1	10.4–10.0 Ma	*Hispanopithecus crusafonti*	Paratype

IPS1818	L M^1	1–2	CP1	10.4–10.0 Ma	*Hispanopithecus crusafonti*	Paratype
IPS1820	L M^2	1–2	CP1	10.4–10.0 Ma	*Hispanopithecus crusafonti*	Paratype
IPS1822	L M$_3$	1	CLL1	9.7 Ma	*Hispanopithecus laietanus*	Invalid holotype of "*Dryopithecus piveteaui*" (nomen nudum)
IPS1826	L M$_2$	1	CV	12.5-11.9 Ma	"*Sivapithecus*" *occidentalis* species inquirenda	Holotype of "*Sivapithecus*" *occidentalis*
IPS1827	L M$_3$	1	CV	12.5-11.9 Ma	"*Sivapithecus*" *occidentalis* species inquirenda	Holotype of "*Sivapithecus*" *occidentalis*
IPS1844	R M^1	1	CLL1	9.7 Ma	*Hispanopithecus laietanus*	—
IPS18000.5	R M^1	4	CLL2	9.6 Ma	*Hispanopithecus laietanus*	—
IPS18000.5	R M^2	2	CLL2	9.6 Ma	*Hispanopithecus laietanus*	—
IPS18000.5	R M^3	1–2	CLL2	9.6 Ma	*Hispanopithecus laietanus*	—
IPS21350	L M^1	1–2	ACM/BCV1	11.9 Ma	*Pieralopithecus catalaunicus*	Holotype
IPS21350	L M^2	1–2	ACM/BCV1	11.9 Ma	*Pieralopithecus catalaunicus*	Holotype
IPS21350	L M^3	2	ACM/BCV1	11.9 Ma	*Pieralopithecus catalaunicus*	Holotype
IPS21350	R M^1	2	ACM/BCV1	11.9 Ma	*Pieralopithecus catalaunicus*	Holotype
IPS21350	R M^2	1–2	ACM/BCV1	11.9 Ma	*Pieralopithecus catalaunicus*	Holotype
IPS35026	L M^1	3	ACM/C3-Ae	11.9 Ma	*Dryopithecus fontani*	—
IPS35026	L M^2	2	ACM/C3-Ae	11.9 Ma	*Dryopithecus fontani*	—
IPS35026	L M^3	1–2	ACM/C3-Ae	11.9 Ma	*Dryopithecus fontani*	—
IPS35027	R M^1	3	ACM/C1-E*	12.3–12.2 Ma	*Anoiapithecus brevirostris*	—

IPS35027	R M^2	1–2	ACM/C1-E*	12.3–12.2 Ma	*Anoiapithecus brevirostris*	—
IPS35027	L M^1	3	ACM/C1-E*	12.3–12.2 Ma	*Anoiapithecus brevirostris*	—
IPS35027	L M^2	1–2	ACM/C1-E*	12.3–12.2 Ma	*Anoiapithecus brevirostris*	—
IPS41734	R M$_2$	1	ACM/BCV4	11.9 Ma	"*Sivapithecus*" *occidentalis* species inquirenda	—
IPS43000	R M^1	1	ACM/C3-Aj	11.9 Ma	*Anoiapithecus brevirostris*	Holotype
IPS43000	R M^2	1–2	ACM/C3-Aj	11.9 Ma	*Anoiapithecus brevirostris*	Holotype
IPS43000	R M^3	1	ACM/C3-Aj	11.9 Ma	*Anoiapithecus brevirostris*	Holotype
IPS43000	L M^1	2	ACM/C3-Aj	11.9 Ma	*Anoiapithecus brevirostris*	Holotype
IPS43000	L M^2	1–2	ACM/C3-Aj	11.9 Ma	*Anoiapithecus brevirostris*	Holotype
IPS43000	L M$_1$	3	ACM/C3-Aj	11.9 Ma	*Anoiapithecus brevirostris*	Holotype
IPS43000	L M$_2$	4	ACM/C3-Aj	11.9 Ma	*Anoiapithecus brevirostris*	Holotype
IPS43000	R M$_1$	3	ACM/C3-Aj	11.9 Ma	*Anoiapithecus brevirostris*	Holotype
IPS58339	L M^2	1	CLL1	9.7 Ma	*Hispanopithecus laietanus*	Likely same individual as IPS58340
IPS58340	L M^3	1	CLL1	9.7 Ma	*Hispanopithecus laietanus*	Likely same individual as IPS58339
MGSB48486	R M^2	1	HP	12.5–9.7 Ma	*Dryopithecus fontani*	—
MGSB25314	L M$_1$	4	TF	10.4–10.0 Ma	*Hispanopithecus crusafonti*	—
MGSB25314	L M$_2$	3–4	TF	10.4–10.0 Ma	*Hispanopithecus crusafonti*	—
MGSB25314	L M$_3$	3	TF	10.4–10.0 Ma	*Hispanopithecus crusafonti*	—

Abbreviations: L, left; R, right; IPS = 'Institut de Paleontologia de Sabadell', former name of Institut Català de Paleontologia Miquel Crusafont; MGSB = Museu de Geologia del Seminari de Barcelona; ACM, local stratigraphic series of Abocador de Can Mata (els Hostalets de Pierola); C3, Cell 3 (ACM sector); BCV, Barranc de Can Vila (ACM sector); CLL, Can Llobateres (Sabadell); CP, Can Poncic (Sant Quirze); CV, Can Vila (els Hostalets de Pierola); HP, Hostalets de Pierola indet. (els Hostalets de Pierola); LT, La Tarumba; TF, Teuleria del Firal (Seu d'Urgell). Numbers after acronyms refer to stratigraphic levels within a single site, whereas other alphanumeric combinations after ACM sectors (separated by a dash) refer to localities within subsectors.

[a] Wear stages are adapted from Smith (1984).

Table 2. Descriptive statistics for relative enamel thickness. The minimum number of individuals (MNI) for each taxon is provided.

Taxon (localities)[a]	2D RET								
	N	MNI	Mean	SD	SE	95% CI	95% CI	Minimum	Maximum
Pierolapithecus catalaunicus (ACM/BCV1)	5	1	15.36	1.15	0.51	14.35	16.37	13.99	16.88
Dryopithecus fontani (ACM/C3-Ae, HP)	3	2	12.33	0.71	0.41	10.56	14.10	11.55	12.95
Anoiapithecus brevirostris (ACM/C3-Aj, ACM/C1-E*)	9	2	14.58	1.35	0.45	13.70	15.46	12.97	17.32
Hispanopithecus crusafonti (CP1, TF)	7	3	14.39	1.26	0.48	13.46	15.33	13.03	16.76
Hispanopithecus laietanus (CLL1, CLL2, LT)[b]	17	5	14.34	2.77	0.67	13.02	15.66	10.35	19.11
"*Sivapithecus*" *occidentalis* (ACM/CV, ACM/BCV4)	3	2	19.66	2.35	1.36	17.01	22.32	17.43	22.11
Taxon (localities)[a]	3D RET								
	N	MNI	Mean	SD	SE	95% CI	95% CI	Minimum	Maximum
Pierolapithecus catalaunicus (ACM/BCV1)	4	1	15.46	2.03	1.02	13.47	17.45	13.24	18.14
Dryopithecus fontani (ACM/C3-Ae, HP)	3	2	11.87	0.93	0.54	10.83	12.92	10.96	12.81
Anoiapithecus brevirostris (ACM/C3-Aj, ACM/C1-E*)	7	2	12.93	1.11	0.42	12.11	13.75	11.40	14.26
Hispanopithecus crusafonti (CP1, TF)	4	2	12.06	1.51	0.76	10.58	13.53	10.97	14.27
Hispanopithecus laietanus (CLL1, CLL2, LT)	10	3	13.46	2.18	0.69	12.11	14.82	10.49	16.38
"*Sivapithecus*" *occidentalis* (ACM/CV)	3	2	18.96	1.74	1.00	16.99	20.92	17.16	20.63

Abbreviations: ACM, local stratigraphic series of Abocador de Can Mata (els Hostalets de Pierola); C3, Cell 3 (ACM sector); BCV, Barranc de Can Vila (ACM sector); CLL, Can Llobateres (Sabadell); CP, Can Poncic (Sant Quirze); CV, Can Vila (els Hostalets de Pierola); HP, Hostalets de Pierola indet. (els Hostalets de Pierola); LT, La Tarumba; TF, Teuleria del Firal (Seu d'Urgell).

[a] Numbers after acronyms refer to stratigraphic levels within a single site, whereas other alphanumeric combinations after ACM sectors (separated by a dash) refer to localities within subsectors.

Table 3. Qualitative dental features of the EDJ of the upper molars.

Features	*P. catalaunicus*	*D. fontani*	*A. brevirostris*	*H. crusafonti*	*H. laietanus*
Dentine horns	little peripheral	little peripheral	little to moderately peripheral	moderately peripheral	very peripheral
Mesial fovea	shallow and moderately developed	shallow and mesially located	deep and restricted	deep and restricted	shallow and restricted
Trigon basin	deeper	shallower	deeper	deeper	shallower
Crista obliqua	high, complete and straight	moderately high and centrally twisted	high, complete and straight	low and often disrupted	moderately high and often disrupted
M^1–M^2 hypocone	aligned with or slightly more lingual than protocone	markedly more lingual than protocone only in M^1	markedly more lingual than protocone	markedly more lingual than protocone	aligned with or slightly more lingual than protocone
Buccolingual waisting	slight	moderate	marked	variable (slight to moderate)	variable (slight to moderate)
Lingual cingulum	slightly developed	moderately developed	well developed	well developed	slightly developed

Table 4. Qualitative dental features of the EDJ of the lower molars.

Features	*H. crusafonti*	*H. laietanus*	*"S." occidentalis*
Metaconid horn	vertical	vertical	tip centrally tilted
Protoconid and entoconid horns	variable but generally peripheral	variable but generally peripheral	less peripheral
Buccal cingulid	well developed	absent to poorly developed	well developed
Lower molar crown waisting	slight	marked	moderate
Tuberculum intermedium (interconulid)	sometimes present	absent	variable
M^2 metaconulid (twinned metaconid)	absent	rarely expressed	marked
Hypoprotocristid and hypometacristid	nearly indistinct and interrupted	nearly indistinct and interrupted	marked, although not merged